Gas Dynamic Limits of the Ram Accelerator

by

Andrew J. Higgins

A thesis submitted in partial fulfillment
of the requirements for the degree of

Master of Science in Aeronautics and Astronautics

University of Washington

1993

Approved by _____

(Chairperson of Supervisory Committee)

Program Authorized
to Offer Degree _____ Aeronautics and Astronautics _____

Date _____

In presenting this thesis in partial fulfillment of the requirements for a Master's degree at the University of Washington, I agree that the Library shall make its copies freely available for inspection. I further agree that extensive copying of this thesis is allowable only for scholarly purposes, consistent with "fair use" as prescribed in the U.S. Copyright Law. Any other reproduction for any purposes or by any means shall not be allowed without my written permission.

Signature _____

Date _____

University of Washington

Abstract

Gas Dynamic Limits of the Ram Accelerator

by Andrew J. Higgins

Chairperson of the Supervisory Committee: Professor Adam P. Bruckner
Department of Aeronautics
and Astronautics

An exploration of the operational envelope of the ram accelerator is presented. The ram accelerator is a novel hypervelocity launcher concept wherein a subcaliber projectile, as it travels through a tube filled with premixed fuel and oxidizer, initiates and sustains a combustion wave, generating continuous thrust. While a quasi-steady, one-dimensional "blackbox" model of the thermally choked ram accelerator accurately predicts the performance, i.e., acceleration, of the projectile, this model says nothing about the regimes of chemistry and Mach number in which the device can operate since it ignores the internal details of the flow. This investigation is motivated by the need for an improved understanding of the stability of the combustion wave on the projectile, which determines the operating limits of the ram accelerator. The simplest model of the flow field of the thermally choked ram accelerator treats the flow over the projectile as isentropic, except for a single normal shock, which is stabilized by thermal choking of the flow behind the projectile due to combustion. This model imposes three gas dynamic limits to operation: a minimum Mach number required to keep the diffuser started, a minimum heat release required to keep the normal shock on the body, and finally a maximum heat release beyond which the normal shock will be driven over the projectile. All three of these limits can be expressed as simple relations of the Mach number (M) of the projectile and the heat release (Q) of the propellant mixture. Together, they define an region of

operation, or "operational envelope," in this Q–M plane. Comparison of this theory to a review of prior experiments with the UW ram accelerator shows the vast majority of experimental operation of the ram accelerator occurs at conditions where a normal shock would have fallen off the base of the projectile. The reason why projectiles cannot operate in more energetic chemistries, where one-dimensional theory predicts they should, is poorly understood. A new series of approximately 30 firings of the ram accelerator is presented to more fully explore the operational envelope of an oxygen/ methane/nitrogen propellant mixture. Both the entrance Mach number of the projectile and the heat release (via dilution) of the propellant were varied to completely map out the experimental envelope of operation. With this improved experimental measurement of limits, modifications to the one-dimensional model are made to investigate the nature of the observed envelope. A simple model of flow separation in overexpanded nozzles implies that the unstart mechanism may be related to high combustion pressures forcing a separation shock past the projectile throat. The results are suggestive of both the limits and ultimate potential of the ram accelerator.

Table of Contents

List of Figures

List of Tables

Nomenclature

A	tube area or annular area between projectile and tube
a	sound speed
c_p	specific heat at constant pressure
F	force on projectile
h	enthalpy per unit mass
M	Mach number
p	pressure
Q	nondimensional heat release
q	heat release per unit mass
R	gas constant
r_{max}	pressure ratio for separation
T	temperature
u	flow velocity

Greek

γ	ratio of specific heats
ρ	density

Subscripts

b	back pressure
s	separation
o	stagnation condition
1	conditions in quiescent gas upstream of the projectile
2	conditions at projectile throat
3	conditions upstream of normal shock
4	conditions downstream of normal shock
5	conditions at projectile base
6	conditions at thermal choke plane
I	back pressure for subsonic choked nozzle
II	back pressure for correctly expanded nozzle
III	back pressure for normal shock at nozzle lip

Acknowledgments

I wish to thank my advisor, Professor Adam P. Bruckner, for his encouragement, his patience, and his granting of complete intellectual freedom, which is hopefully reflected in the eclectic nature of this study. Professor Abraham Hertzberg in a singular act of prescience proposed the ram accelerator concept ten years ago; fulfillment of that vision has been the motivation for this work. Professor David T. Pratt was an unquenchable source of discussion on supersonic combustion and the role of separation in scramjet isolators. Dr. Carl Knowlen was instrumental in this experimental series, from planning to execution, and provided a healthy amount of intellectual sparring along the way.

A silent "thank you" goes to the graduate students who endured my tenure: Jacqueline Auzias de Turenne, Edward Burnham, Gilbert Chew, Barbrina Dunmire, John Hinkey, and Matthew Jardin. Of these, special appreciation is expressed to Mr. Burnham, for his wonderful data extraction software, Mr. Hinkey, whose assistance with the gas chromatography kept this study out of *The Journal of Irreproducible Results*, and Mr. Jardin, for never shying away from deliberations, technical and otherwise, which often ran well into the morning. All my fellow students are acknowledged for their general *esprit de corps* under often difficult conditions.

Malcolm Saynor masterfully fabricated the projectiles required in a shot-intensive investigation, without which this work would have remained mere theoretical ruminations on paper.

Finally, deep appreciation is expressed to my friend, Lieutenant Jeffrey Schavland, whose penchant for grammar and usage was invoked in several eleventh hour reviews of papers and reports in the development of this thesis.

I. Introduction

Since 1983 research has been carried out at the University of Washington (UW) on a hypervelocity launcher concept called the ram accelerator.[1] The device is similar to a conventional ramjet, with the outer cowling replaced by a stationary tube, and a projectile which resembles the centerbody of a ramjet (Fig. 1.1). The tube is filled to high pressure (5-50 atm) with a premixed propellant mixture, usually oxygen, methane, and diluent gases. The projectile is injected into the tube at supersonic velocities by a light gas gun. The resulting shock structure initiates and sustains a combustion wave which accelerates the projectile down the tube. Hence, the
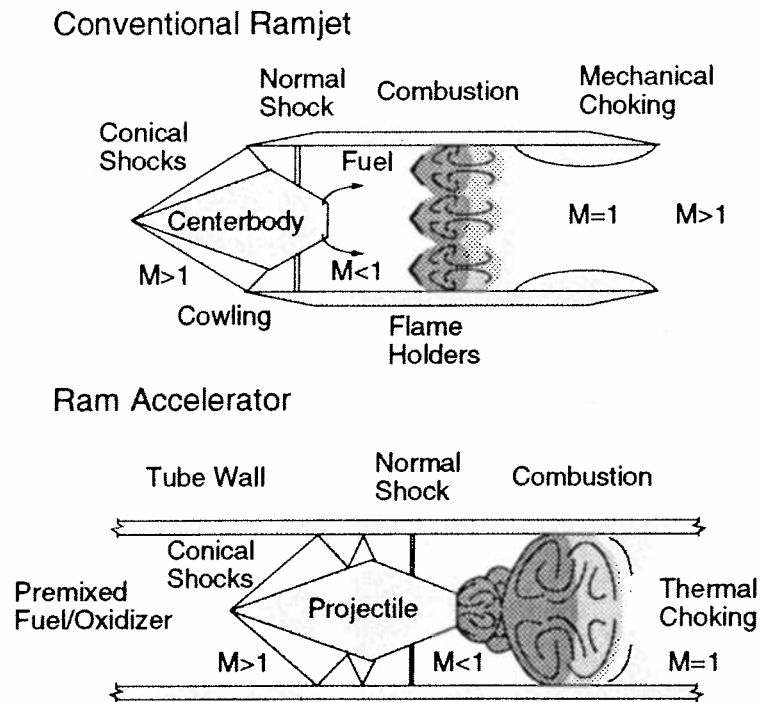
Fig. 1.1   Supersonic airbreathing ramjet and the thermally choked ram accelerator.

Conventional Gun
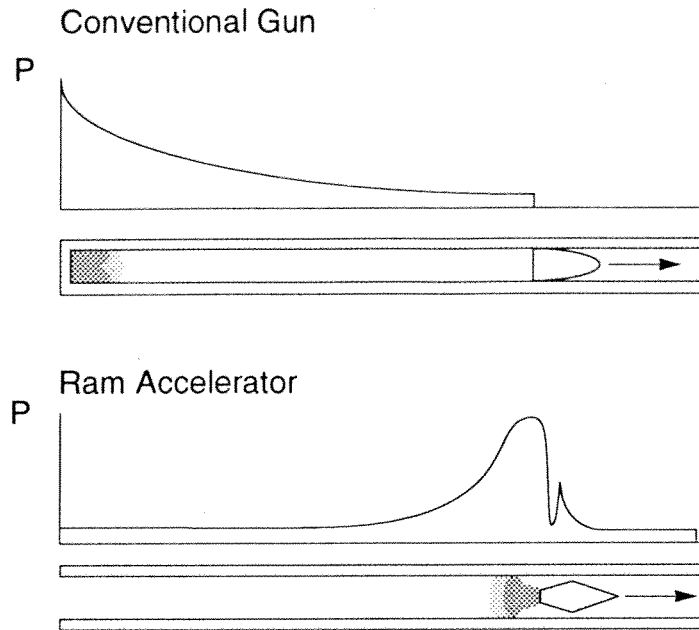
Ram Accelerator

Fig. 1.2   Pressure distributions in a conventional
gun and the ram accelerator.

highest pressures in the tube are in the vicinity of the projectile, as compared
to a conventional launcher where the highest pressures are in the breech
(Fig. 1.2). The ram accelerator at the UW facility has accelerated 60-90 gm
projectiles to velocities of 2.7 km/sec in a 16 m tube. While the present facility
is only a 38 mm internal diameter tube, the ram accelerator holds great
scaling potential for applications in surface-to-orbit launching[2] and ground-
based testing of hypersonic propulsive cycles.[3] This potential for scaling has
been recently realized by efforts at the U.S. Army Research Laboratory
(ARL)[4] and the French-German Research Institute (ISL).[5]

Many modes of ram accelerator propulsion have been suggested,[1,6] but
the emphasis of experimental work to date has been on the thermally choked
mode,[7] shown in Fig. 1.1. In this mode, a shock system is stabilized on the

body by thermal choking via subsonic combustion in the full tube area behind the projectile. The incoming flow is first compressed by a system of oblique and normal shocks, neither of which is strong enough to initiate combustion. Beyond the thermal choke point, an unsteady expansion occurs, which is gas dynamically decoupled from the projectile. As the projectile accelerates, the normal shock recedes along the body until it falls off the base of the projectile and occupies the full tube area. For a projectile base which tapers to a point, the projectile velocity at which the shock falls off and ceases to provide thrust can be shown to equal the Chapman-Jouguet (CJ) detonation speed of the mixture.[1]

In practice, it has been found that the projectile can accelerate through the CJ detonation speed of a particular mixture. This "transdetonative" phenomenon was an unexpected experimental result and is believed to result from partial heat addition occurring on the projectile body. Whether this ignition is caused by shocks, shock-boundary layer interactions, or reactions in the boundary layer, it is believed to result in a "combined cycle" in which some heat is released on the body and some in the recirculation zone behind it.

Transdetonative operation allows the projectile to accelerate to superdetonative speeds, where again various propulsive modes are possible. One of the modes of significant interest involves igniting the propellant mixture with a reflected oblique shock, similar to the oblique detonation wave engine. In these superdetonative modes, the flow over the projectile remains supersonic and the heat release occurs in the annular region between the projectile and tube wall.

These various regimes of operation can be classified by the speed of the projectile relative to the CJ speed of the mixture. The subdetonative regime,
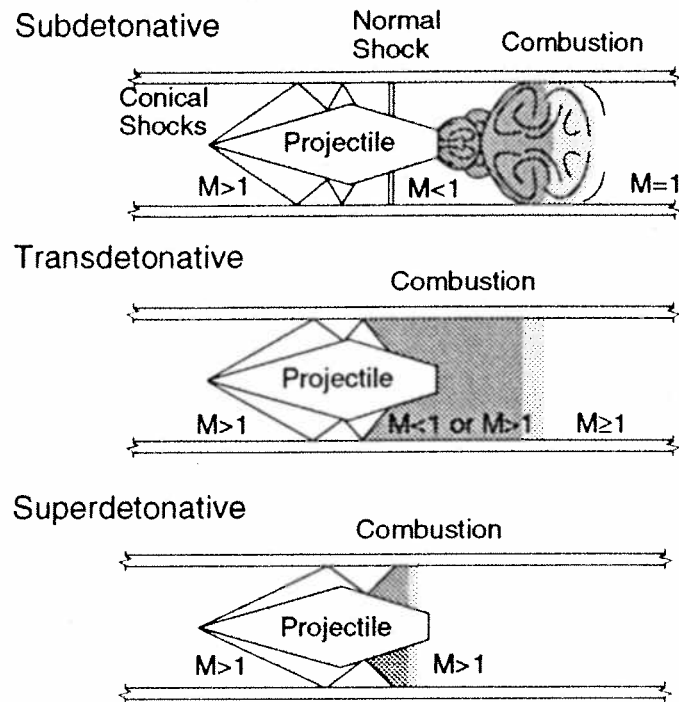
Fig. 1.3   Flow   fields   associated   with   different
regimes of operation.

where the flow is believed to thermally choke behind the projectile, occurs at speeds less than 90% of the CJ detonation speed.   The transdetonative velocity regime refers to projectile speeds between 90% and 110%, while the superdetonative is above 110% of the CJ detonation speed. Schematics of the flow fields associated with each regime are illustrated in Fig. 1.3.

While   considerable   effort   has   been   directed   at   predicting   the performance of these various modes, little work has been done to determine their   operational   limits.   Moreover,   the   conditions   under   which   the combustion will overtake the projectile or will fall-off the base are poorly understood. This investigation is motivated by the need for an improved understanding of the gas dynamic phenomena which limit the operation of the

ram accelerator, particularly in the subdetonative and transdetonative regimes.

II. Theoretical Considerations

Of the modes outlined in Chapter I, only the thermally choked mode is amenable to a closed form, analytic solution. In this chapter, two models will be presented. The first is a "blackbox" model which ignores the details of the flow but is able to predict the thrust. The second model attempts to fill in the processes between the undisturbed flow upstream of the projectile and the thermal choking plane downstream of the projectile in order to determine the theoretical limits to operation.

2.1 The "Blackbox" Model

Once the assumption of a thermally choked flow in the full tube area behind the projectile has been made, the thrust on the projectile is uniquely determined by the flow conditions upstream of the projectile and at the thermal choke point. If the flow at the thermal choke point is assumed to be in equilibrium, the conditions can be determined by an equilibrium chemistry combustion routine. This model of the ram accelerator can be thought of as a
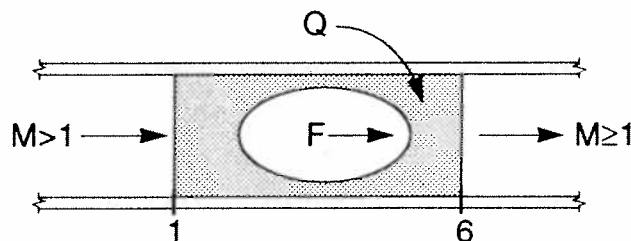
Fig. 2.1   Control volume for the "blackbox" model
of the ram accelerator.

"blackbox," since it ignores the details of the flow and considers only the conditions at the entrance and exit planes of the projectile control volume.

Beginning with the conservation of momentum

$$F = p_6 A_6 - p_1 A_1 + u_6^2 \rho_6 A_6 - u_1^2 \rho_1 A_1 \qquad (2.1)$$

a nondimensional thrust parameter can be defined as

$$\frac{F}{p_1 A} = \frac{p_6}{p_1} - 1 + M_6^2 a_6^2 \frac{\rho_6}{p_1} - M_1^2 a_1^2 \frac{\rho_1}{p_1} \qquad (2.2)$$

where the definition of Mach number, $M = u/a$ has been used. Using an ideal equation of state ($p = \rho RT$) and the relation for sound speed ($a = (\gamma RT)^{1/2}$), this relation can be simplified to

$$\frac{F}{p_1 A} = \frac{p_6}{p_1} (1 + \gamma_6 M_6^2) - (1 + \gamma_1 M_1^2) \qquad (2.3)$$

Applying the same assumptions to the conservation of mass

$$\rho_1 u_1 A_1 = \rho_6 u_6 A_6$$

we obtain

$$\frac{p_6}{p_1} = \frac{M_1}{M_6} \sqrt{\frac{\gamma_1 R_6 T_6}{\gamma_6 R_1 T_1}} \qquad (2.4)$$

Starting with the conservation of energy

$$h_1 + \frac{u_1^2}{2} + \Delta q = h_6 + \frac{u_6^2}{2}$$

and nondimensionalizing by the value $c_{p1}T_1$ allows the introduction of the heat release parameter $Q = \Delta q / (c_{p1}T_1)$, also known as the second Damköhler parameter.

$$\frac{h_1}{c_{p1}T_1} + \frac{\gamma_1 - 1}{2}M_1^2 + Q = \frac{h_6}{c_{p1}T_1} + \frac{\gamma_6 - 1}{2}M_6^2\left(\frac{c_{p6}T_6}{c_{p1}T_1}\right)$$

Of course, for a calorically perfect gas ($h = c_p T$ with c_p = constant), the above relation simplifies considerably. However, for a high temperature, chemically reacting flow, the assumption of a calorically perfect gas is a poor one. Hence, all terms will be kept for now. Solving for the ratio of static temperatures

$$\frac{T_6}{T_1} = \frac{c_{p1}}{c_{p6}}\left[\frac{\dfrac{h_1}{c_{p1}T_1} + \dfrac{\gamma_1 - 1}{2}M_1^2 + Q}{\dfrac{h_6}{c_{p6}T_6} + \dfrac{\gamma_6 - 1}{2}M_6^2}\right] \tag{2.5}$$

Substituting Eq. 2.5 into Eq. 2.4, the relation for the ratio of static pressures can be substituted into Eq. 2.3, yielding the thrust equation

$$\frac{F}{p_1 A} = \frac{M_1 \gamma_1}{M_6 \gamma_6}\sqrt{\left(\frac{\gamma_6 - 1}{\gamma_1 - 1}\right)\frac{\dfrac{h_1}{c_{p1}T_1} + \dfrac{\gamma_1 - 1}{2}M_1^2 + Q}{\dfrac{h_6}{c_{p6}T_6} + \dfrac{\gamma_6 - 1}{2}M_6^2}}\,(1 + \gamma_6 M_6^2) - (1 + \gamma_1 M_1^2) \tag{2.6}$$

Assuming that the flow thermally chokes at station 6, the thrust equation can be written as

$$\frac{F}{p_1 A} = M_1 \frac{\gamma_1}{\gamma_6} \sqrt{\left(\frac{\gamma_6 - 1}{\gamma_1 - 1}\right) \frac{\dfrac{h_1}{c_{p1} T_1} + \dfrac{\gamma_1 - 1}{2} M_1^2 + Q}{\dfrac{h_6}{c_{p6} T_6} + \dfrac{\gamma_6 - 1}{2}} (1 + \gamma_6) - (1 + \gamma_1 M_1^2)} \qquad (2.7)$$

The assumption of thermal choking is largely validated by the excellent agreement between the predicted and observed values of projectile acceleration, although arguments for this condition can be made on entirely theoretical grounds, since it corresponds to a state of maximum entropy.[8] In practice, this equation is rarely used; the conditions at station 6 are determined via a chemical equilibrium code, allowing thrust to be directly computed in terms of the "primitive" variables p, h, T, u, etc.[9] Comparisons for the acceleration observed experimentally and predicted via an equilibrium calculation of the thrust will be presented later in this chapter.

If the gas is assumed to be locally calorically perfect (*i.e.*, $h_i = c_{pi} T_i$ at state i only), the thrust equation above considerably simplifies to

$$\frac{F}{p_1 A} = M_1 \frac{\gamma_1}{\gamma_6} \sqrt{2 \left(\frac{\gamma_6^2 - 1}{\gamma_1 - 1}\right) (1 + \frac{\gamma_1 - 1}{2} M_1^2 + Q) - (1 + \gamma_1 M_1^2)}$$

which is the form of the thrust equation appearing in Refs. 1 and 7. It is unlikely, however, that a gas could be locally calorically perfect without having a constant c_p. In general, a constant c_p implies a constant γ as well. Hence,

this form of the thrust equation is not entirely thermodynamically consistent. The $h/c_p T$ terms in Eq. 2.7 must be maintained as a measure of the caloric imperfection at stations 1 and 6.

If a constant γ is assumed, further simplification yields

$$\frac{F}{p_1 A} = M_1 \sqrt{\frac{(\gamma-1)M_1^2 + 2(Q+1)}{\gamma+1}}\,(1+\gamma) - (1+\gamma M_1^2) \qquad (2.8)$$

If we expand out this expression to

$$\frac{F}{p_1 A} = M_1 \sqrt{\frac{(\gamma-1)M_1^2 + 2(Q+1)}{\gamma+1}} + \gamma M_1 \sqrt{\frac{(\gamma-1)M_1^2 + 2(Q+1)}{\gamma+1}} - 1 - \gamma M_1^2$$

each term can be show to correspond to each of the four terms in the original momentum equation (Eq. 2.3), allowing an estimate of the magnitude of the different forces acting on the control volume. Over the nominal range of Q and M

$$p_1 \ll p_6 \approx \frac{\rho_6 u_6^2}{\gamma} < \rho_1 u_1^2$$

Hence, the pressure term at the inlet is insignificant compared to the momentum flux at the inlet and the forces at the exit plane. It is interesting to note that the ram accelerator gets substantial thrust from *both* the pressure and momentum flux at the exit plane, unlike a conventional jet or
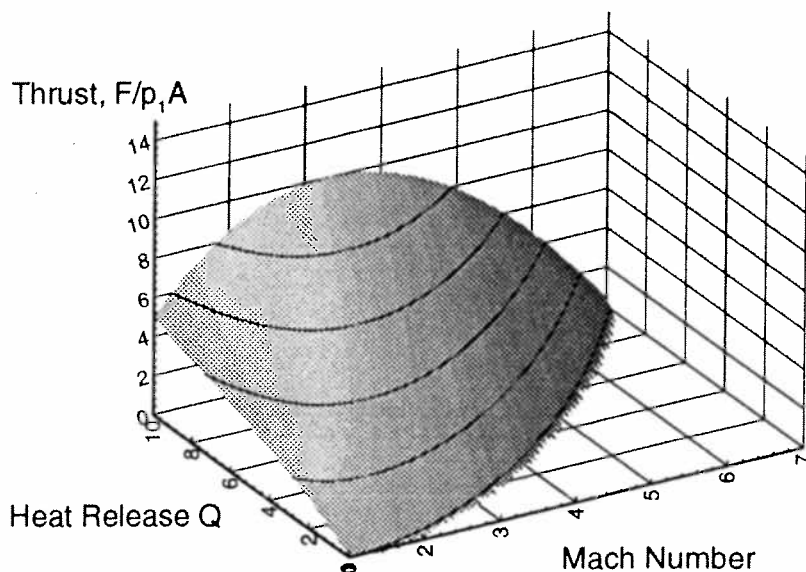
Fig. 2.2 Thrust as a function of heat release Q and
Mach number for $\gamma = 1.4$.

rocket. These respective forces are, in fact, related by γ.

The various forms of the thrust equation developed above are functions of the flight Mach number M_1 and the heat release, Q, with a mild dependence on the thermodynamic properties at the entrance and exit planes. The thrust coefficient is plotted as a surface above the Q–M plane in Fig. 2.2 for a calorically perfect gas (Eq. 2.8). If the equation for the thrust coefficient is equated to zero, the resulting relation between Q and M is exactly the rule of Chapman and Jouguet, which confirms the earlier statement that the thrust of a thermally choked ram accelerator goes to zero as the projectile velocity approaches the detonation speed of the mixture. Hence, the intersection of

the thrust surface on the Q–M plane plotted in Fig. 2.2 defines the Chapman-Jouguet relation.

The thrust equation can also be derived as part of a generalized Hugoniot analysis, with the addition of a force component not included in the classical Hugoniot equations.[8] Such analysis strongly reinforces the idea that the performance of the thermally choked ram accelerator is independent of the details of the internal flow field.

While this "blackbox" model is excellent at predicting performance, it says nothing about the ability of the ram accelerator to operate at a given velocity or in a given mixture. This is to say, *if* a ram accelerator projectile successfully stabilizes the combustion process, the model presented above will accurately reproduce its performance, but it will not be able to determine if the projectile can successfully drive at all. To determine the limits to operation, the details of the flow field must be examined.

2.2 A One-Dimensional Flow Field Model

The simplest model of the thermally choked ram accelerator flow field treats the flow over the projectile as isentropic, except for a single normal shock (Fig. 2.3). In reality, a single normal shock is unlikely; the flow more closely resembles the complex system of normal and oblique shocks observed in supersonic flow in long ducts.[10] This shock on the body is stabilized by the thermal choking of the flow in the full tube area behind the projectile. The combustion behind the projectile is modeled as Rayleigh flow. The normal shock is free to move in response to changing upstream and downstream conditions. As the projectile accelerates, the normal shock recedes until it
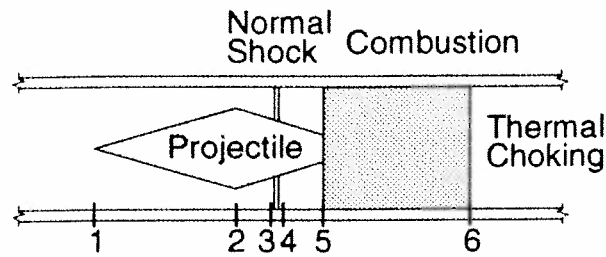
Fig. 2.3   One-dimensional model of the thermally
choked ram accelerator flow field.

reaches the base of the projectile.   If the projectile base were tapered to a
point, the normal shock would eventually reach the full tube area as the
projectile is accelerated to the CJ detonation speed.   This results in the
cessation of thrust, making the CJ speed the maximum theoretical velocity of
thermally choked operation, which concurs with the results of the "blackbox"
analysis presented in the previous section.

Such a model imposes three limits on ram accelerator operation.   First,
the   projectile   must   maintain   a   certain   minimum   Mach   number
(approximately 2.5 for projectile geometries used in the UW facility) to keep
the flow supersonic past the throat (station 2 in Fig. 2.3).   Below this Mach
number, the flow will choke on the projectile forebody, resulting in an
"unstart." Second, a certain maximum is imposed on the heat release of the
mixture, beyond which the normal shock is disgorged from the throat, also
resulting in a unstart. Finally, a certain minimum heat release is required to
keep the shock wave from falling off the projectile base.   All three of these
limits can be expressed as simple relations of the Mach number of the
projectile and the heat release of the propellant mixture (along with the
thermodynamic properties of the gaseous mixture, such as the specific heat
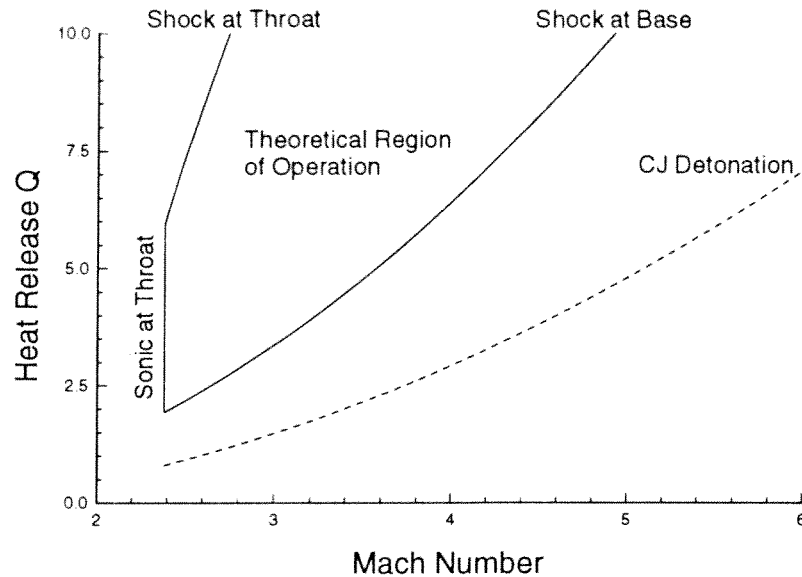
Fig. 2.4   Theoretical operational envelope of the
ram accelerator.

ratio). For a given projectile throat-to-tube and base-to-tube area ratio, these
relations define a theoretical region of operation, or operational envelope, for
the ram accelerator. This envelope, for the nominal UW geometry, is shown in
a plot of heat release vs. projectile Mach number in Fig. 2.4, along with a
curve indicating the dependence of the CJ Mach number on Q. As mentioned
before, for a projectile whose base tapers to a point, the shock-at-base
condition coincides with the CJ curve. For Fig. 2.4, the gas was assumed to be
calorically perfect, with the specific heat ratio γ taken as a constant 1.4.
Hence, in this example the flow is treated as an inert working fluid with some
kind of external heat addition. Modifications can be included in this one-
dimensional model to account for losses in the diffuser and across the
projectile blunt base, but the changes are minor and do not affect the
qualitative nature of the envelope.[9]

Theoretical Region
of Operation

Thrust, F/p₁A

Heat Release Q
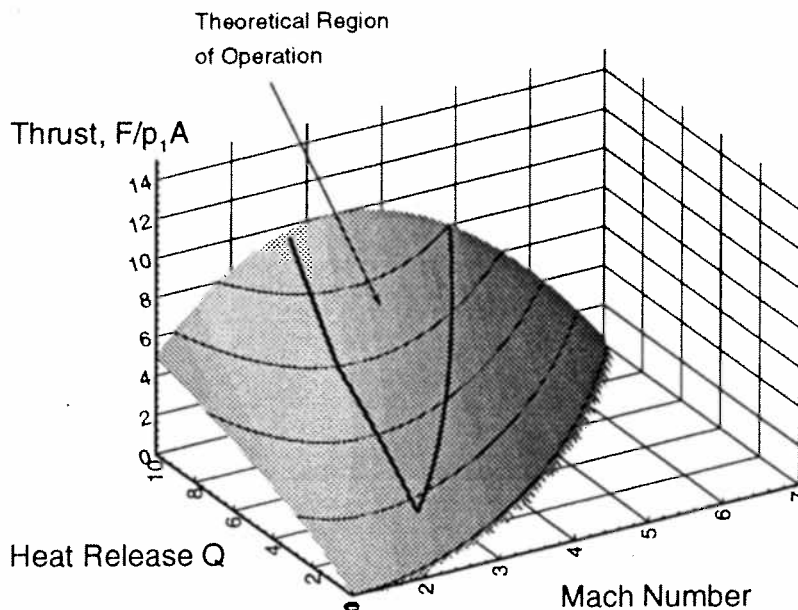
Mach Number

Fig. 2.5   Theoretical operational envelope projected
onto the thrust surface (*cf.* Fig. 2.2).

This envelope bounds a large region of Mach number and heat release
values, indicating that a potentially wide range of operating conditions might
be realized.   Moveover, the theoretical envelope in Fig. 2.4 can be projected
onto the thrust surface from the previous section (Fig. 2.2), as seen in Fig. 2.5.
This is a promising result; not only does the "blackbox" analysis predict high
values of thrust, a one-dimensional model suggests the ram accelerator should
be able to access these regions of high thrust.

This model is also a convenient way to examine the influence of various
nonideal flow effects, such as precombustion on the projectile.   For example,
let us arbitrarily prescribe 10% of the total heat release to occur at the
projectile throat (station 2 in Fig. 2.3), perhaps as the result of combustion
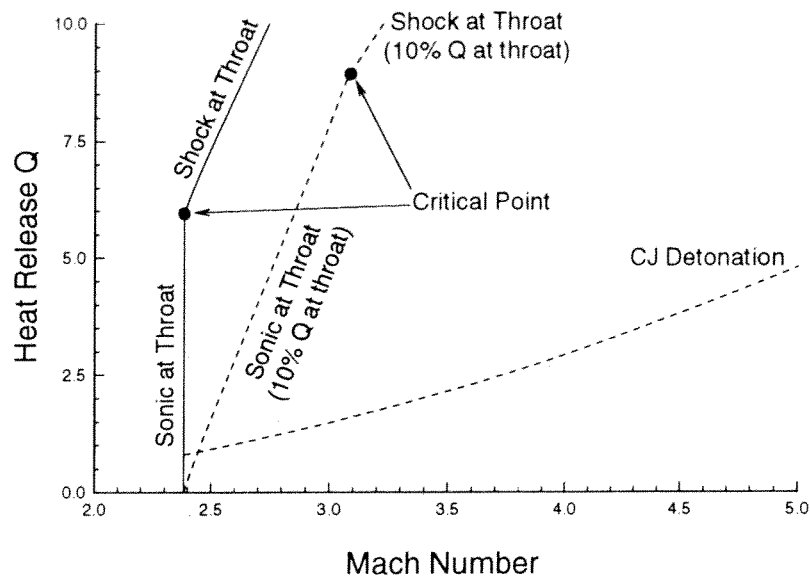
Fig. 2.6   The effect on the operational envelope of a
10% release of the total Q at the throat.

occurring on the blunt leading edge of the projectile fin.   Of course,
determining the actual heat release due to premature ignition would require
detailed chemical kinetic and flow considerations. The effect this has on the
theoretical envelope is shown in Fig. 2.6.   Note that the minimum Mach
number for operation at both the sonic-at-throat and shock-at-throat limits
has been raised. This is to say, precombustion has the effect of driving the
flow toward sonic, allowing the area contraction at the throat to more easily
choke the flow. Precombustion also moves the normal shock forward, allowing
it to be disgorged from the throat at lower values of total heat release. The
fact that *both* these unstart mechanisms can be relevant will be of importance
later when we attempt to determine the nature of the actual limits to the ram
accelerator.

It is also important to point out that the location of the heat addition on the forebody must be specified. For example, if 10% of the total Q were prescribed to be released at the projectile nose tip, as opposed to the throat, the precombustion would have a different, more pronounced effect on the operational envelope. This is in sharp contrast to the considerations in the previous section, where the location of the heat addition, or the flow processes in general, inside the "blackbox" did not appear in the analysis. Why should the conditions required to choke the flow at the throat or disgorge the normal shock be sensitive to the location of the heat release, while the thrust is not? Moreover, why is a control volume enclosing station 1 to 2 path dependent, while a control volume analysis from station 1 to 6 is path *independent*? In the previous section, the derivation of the thrust equation exploited the integral relation[10]

$$\frac{p_6}{p_1} = \frac{M_1 A_1}{M_6 A_6} \sqrt{\frac{1 + \frac{\gamma - 1}{2} M_1^2}{1 + \frac{\gamma - 1}{2} M_6^2} \left(\frac{Q}{1 + \frac{\gamma - 1}{2} M_1^2} + 1 \right)} \tag{2.9}$$

This equation, when M_6 is set to unity and Q and M_1 are assumed to be known, provides a closed form solution for the ratio of the static pressures, which is directly related to the thrust coefficient via Eq. 2.3 in the previous section. For heat addition to a constant area flow, where the exit Mach number is not known *a priori*, Eq. 2.9 also yields a closed set, since a (frictionless) constant area section cannot support a difference in stream

thrust:

$$\left(\frac{p_6}{p_1}\right)_{\text{ConstantArea}} = \frac{1 + \gamma M_1^2}{1 + \gamma M_6^2}$$

For heat addition with area change, however, there is no equivalent integral expression to provide a closed set of equations. The momentum equation cannot be used, since the force on the section walls (the nose cone, in this case) is unknown. One must specify the entire history of the flow processes through the control volume to determine the end state.

With this path dependence firmly established, the question remains what is the effect of different paths, *i.e.*, where does heat addition produce the most pronounced effects on the flow field. These questions are answered most easily by examining the differential relation of total pressure to total temperature[10]

$$\frac{dp_o}{p_o} = -\frac{\gamma M^2}{2}\frac{dT_o}{T_o}$$

Hence, total temperature changes at high Mach number have a more significant effect on the stagnation pressure than at low Mach numbers. This means that heat addition to regions of flow at higher Mach number, such as the nose, has a greater influence on the flow at the throat. Also, since the total decrease in the stagnation pressure is dictated by the requirements of thermal choking, the normal shock must becoming weaker by moving upstream in response to the decrease in the stagnation pressure caused by precombustion.[9] Hence, heat addition to regions of flow at higher Mach number has a more significant effect on the normal shock's location than at
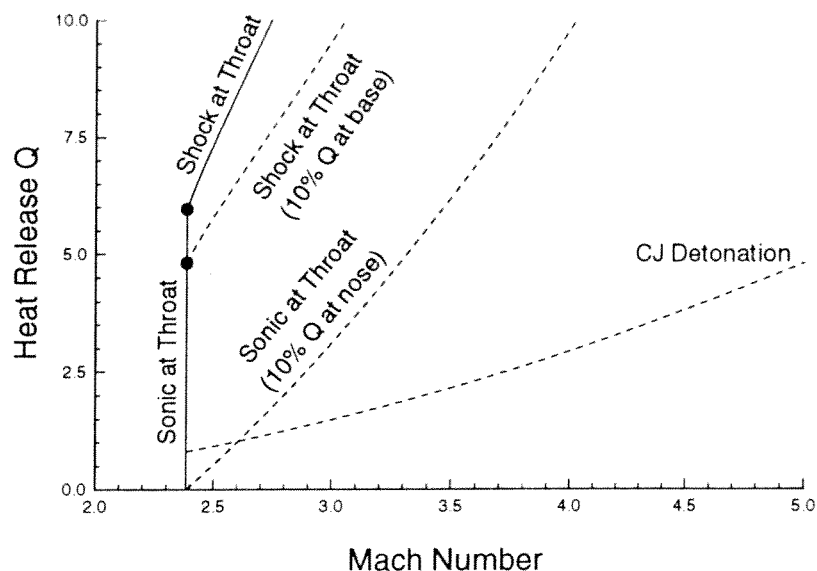
Fig. 2.7   The effect on the operational envelope of a
10% release of the total Q at the nose and
base.

lower Mach numbers.

For example, we will again prescribe 10% of the total heat to be released prematurely, as was done in Fig. 2.6, only now the heat release will occur at station 1, where the flow is at the full flight Mach number. The effect this precombustion has on the operational envelope is shown in Fig. 2.7. Note that the sonic-at-throat minimum Mach number limit is increased even further and the critical point, where the shock-at-throat mechanism takes over, is no longer visible. Also shown in Fig. 2.7 is the effect of 10% heat release at the projectile base, immediately upstream of station 5, where the flow has been decelerated to subsonic. This precombustion has no way to choke the flow at the throat, of course, and has only a minor influence on the
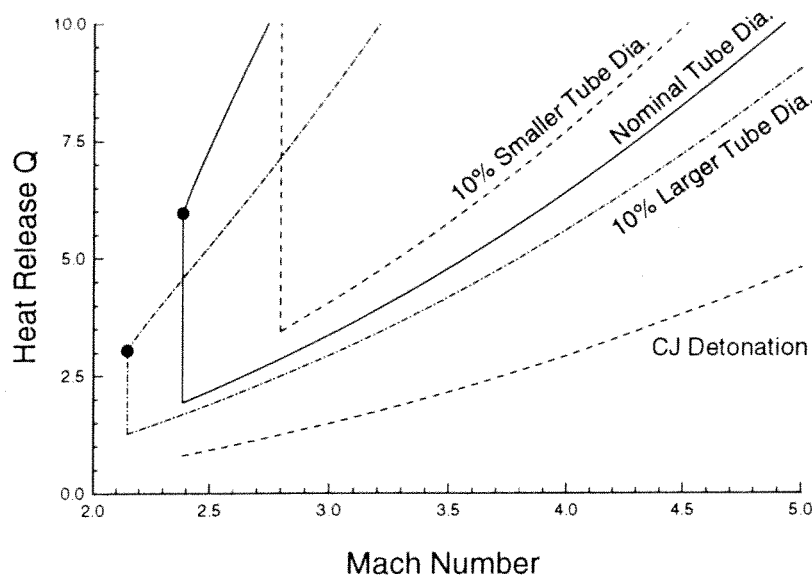
Fig. 2.8 The effect on the operational envelope of
varying the tube diameter.

normal shock location, demonstrating the minimal effect of subsonic heat
addition.

Finally, this simple, one-dimensional model can be used to examine the
effects of area change on the operational limits. Fig. 2.8 shows the effect of
increasing and decreasing the tube diameter by 10% from the nominal value
for the UW ram accelerator. These changes could also correspond to changing
the projectile's throat and base diameter by an equivalent amount. Reducing
the tube diameter increases the minimum Mach number required to start the
projectile diffuser, but this tighter throat area increases the amount of heat
release required to drive the normal shock over the projectile. Increasing the
tube area has the opposite effects. If which of the two unstart mechanisms
responsible for limiting actual operation can be identified, then varying the

throat-to-tube area ratios accordingly could increase the observed operational envelope.

2.3 Comparison to Experiment

Although these theoretical considerations suggest the ram accelerator has a wide envelope of operation, experimentally it is unable to access most of the operational region that the simple model predicts. Shown in Fig. 2.9 are the results of two different firings of the UW ram accelerator, which are typical of the experiments performed to date. Velocity-distance data are presented from a single stage (*i.e.*, a single propellant mixture) experiment which exhibited transdetonative operation. The propellant mixture used is indicated in Fig. 2.9(a) and the initial fill pressure was 25 atm. The second experiment is an example of staging, where the propellant mixture is tailored down the length of the tube to accelerate the projectile continuously at subdetonative velocities while maintaining high accelerations. In this multistage experiment, the initial fill pressure was 45 atm for all four stages. The projectile masses were 63 and 80 gm respectively. The corresponding theoretical curves (generated by the "blackbox" analysis) are in good agreement with the experimental results while the projectile is operating below ~90% of the CJ speed.

Although the theoretical envelope shown in Fig. 2.9(b) shifts slightly for the different thermodynamic properties of each mixture, the changes are too subtle to show in this figure. The fact that the single stage experiment exhibited transdetonative performance, while the multistage experiment remained subdetonative, is easily seen in the Q–M plane. We can see from
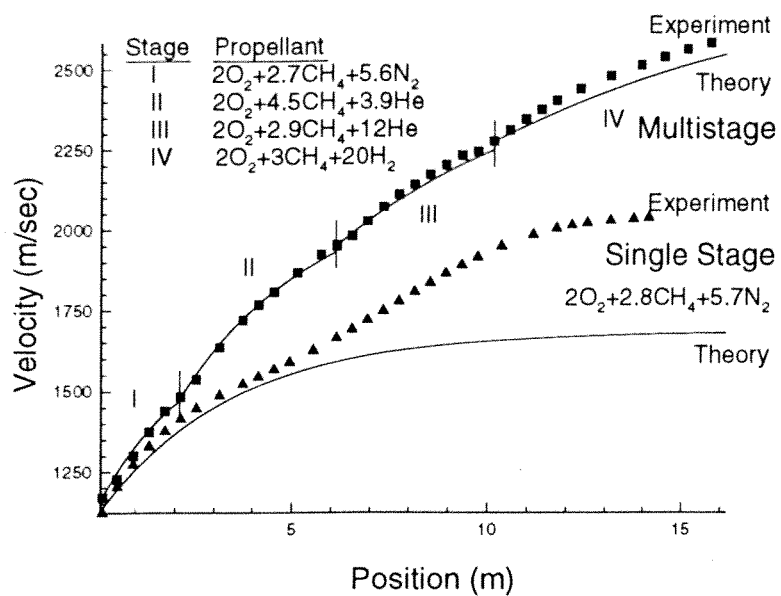
(a)
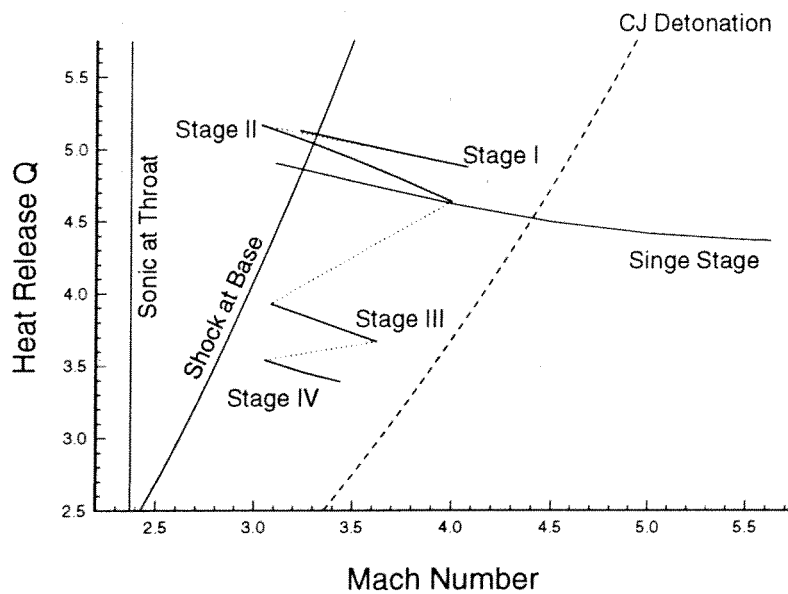
(b)

Fig. 2.9 Two experimental firings showing (a) velocity-distance profiles and (b) a comparison with the theoretical operating limits.
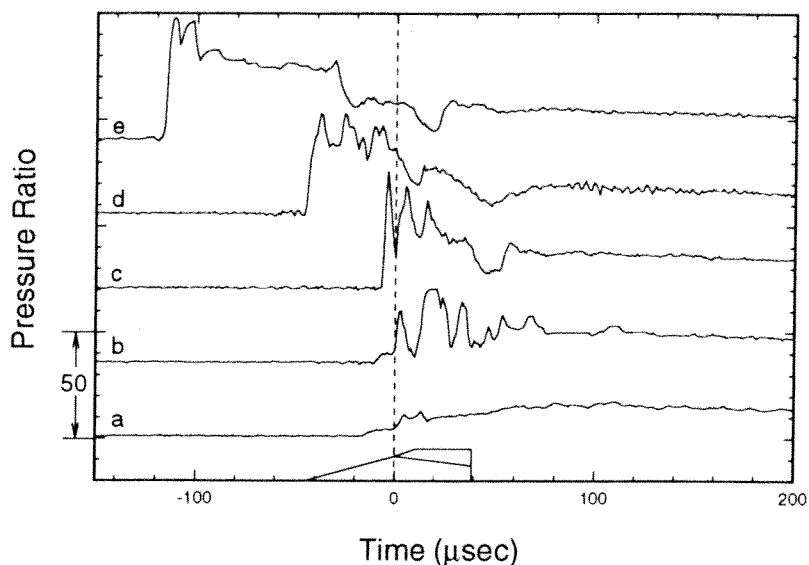
Fig. 2.10 Evolution of an unstart as seen by tube
wall mounted pressure transducers.

these plots that, for the most part, the ram accelerator typically operates at conditions under which a normal shock would have fallen off the base of the projectile.

While attempts have been made to operate in more energetic mixtures, which should exhibit higher acceleration, these experiments often result in an almost immediate unstart of the projectile. An unstart is a very violent phenomenon in which a normal shock is disgorged from the throat of the projectile, often developing into an overdriven detonation wave that propagates down the tube in front of the projectile. This irrevocable phenomenon causes a pronounced deceleration of the projectile and often results in its complete structural collapse. The pressure profiles of such an unstart, normalized by the fill pressure, are shown in Fig. 2.10. Trace "a" in Fig. 2.10 indicates a pressure profile of the flow field while the projectile is in

nominal operation at a velocity of 1800 m/sec. A scaled outline of a projectile shows its relative size. The spikes seen near the throat result from the conical bow shock reflecting between the projectile and the tube wall. The elevated pressure region behind the projectile is the result of the heat release from combustion. The remaining traces (b-e) show the progression of an unstart, taken from pressure transducers 0.4 m apart. A very large pressure spike (pressure ratio of ~50) is seen developing at the throat and propagating in front of the projectile, eventually evolving into an overdriven detonation wave. The total time lapse for the records shown in Fig. 2.10 is ~1 msec.

The actual mechanism of these unstarts, which limit the operation of the ram accelerator, is poorly understood. As mentioned previously, precombustion could choke the flow at the throat of the projectile, or the heat release could drive the shock system over the projectile. The observed operational limits and the nature of these limiting mechanisms are the subjects of this investigation. For a single class of propellant mixture, the operational envelope is explored by varying the energetics of the propellent mixture and the entrance Mach number of the projectile.

III. Experimental Facility and Procedure

The ram accelerator facility consists of a light gas gun, ram accelerator test section, final dump tank, and projectile decelerator. The 38 mm bore, 6-m-long single-stage light gas gun is used to accelerate the projectile to a velocity sufficient to maintain supersonic flow past the projectile throat, usually around 1.1 km/sec. The 16-m-long ram accelerator test section consists of eight 2-m-long, high-strength steel tubes having a bore of 38 mm and an outer diameter of 102 mm. The ram accelerator section is designed to operate at propellant fill pressures up to 50 atm. There are 40 equidistant multiple-port instrument stations at 40 cm intervals along the test section of the ram accelerator. Thin Mylar diaphragms close off each end and separate different mixtures in multistage experiments. A more detailed description of the facility is presented in Ref. 7.
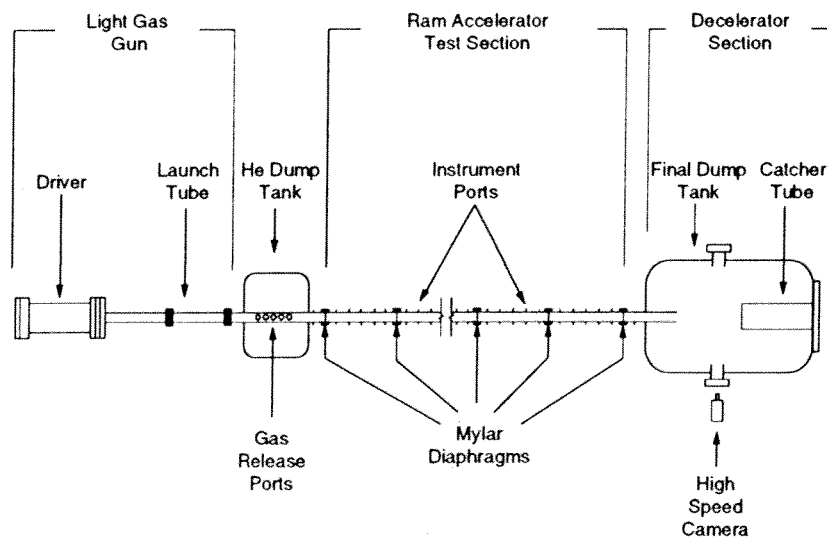
Fig. 3.1   University of Washington ram accelerator
           facility.
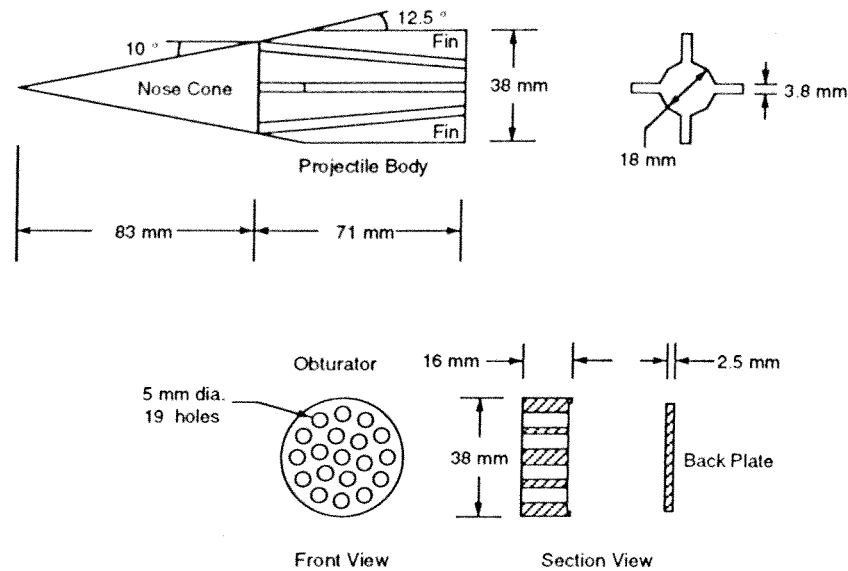
Fig. 3.2   Ram accelerator projectile and obturator.

A schematic of the projectile geometry used in these experiments is shown in Fig. 3.2. The projectiles were fabricated from magnesium alloy in two hollow pieces (nose cone and body), which thread together at the throat. The octagonal cross section of the body is a machining convenience. The fins are required to center the projectile in the tube. The projectiles used in this series of experiments had a mass of 64 gm.

3.1 Propellant Selection

The theoretical operational envelopes for the thermally choked ram accelerator derived in the previous chapter are functions exclusively of the projectile Mach number and the heat release. To explore the corresponding experimental operational envelope, the heat release must be varied in a systematic way. Specifying the heat release, however, does not uniquely

specify the chemistry of the propellent mixture. For example, a stoichiometric mixture of oxygen and methane ($2O_2$ + CH_4) has a nondimensional heat release parameter Q of 19.8 if the flow is thermally choked at a projectile Mach number of 4. Suppose we wish to explore a mixture with a Q value of 5.0. We could add excess fuel to dilute the mixture, yielding a mixture of $2O_2$ + $6.3CH_4$, or add an inert gas like nitrogen, giving $2O_2$ + CH_4 + $15N_2$. Hence, to uniquely relate a propellant mixture to a value of heat release, we must constrain our choice of mixture in some way.

For this series of experiments, the fuel equivalence ratio was fixed to 2.8 while varying the amount of nitrogen dilution ($2O_2$ + $2.8CH_4$ + XN_2). The selection of this chemistry was not made in complete capriciousness. A similar class of mixture ($2O_2$ + $2.8CH_4$ + $5.7N_2$) has proven a reliable first stage in the operation of the UW facility and routinely exhibits transdetonative performance (see Fig. 2.9). In the experiments presented here, the amount of nitrogen dilution was varied from 3 to 12 moles, or 40% to 70% by volume. The heat release parameter Q as a function of this dilution at various projectile Mach numbers is shown in Fig. 3.3. The heat release decreases with increasing projectile Mach number for a given mixture due to the increased static temperature at the plane of thermal choking, resulting in greater dissociation losses. This loss is visible in plots of experimental data in the Q–M plane as a slight downward slope of the experimental curve, as seen in Fig. 2.9(b). With the aid of Fig. 3.3, the heat release can be uniquely related to the mixture composition, and vice versa, for any data from the experimental series presented in this thesis.

It should be emphasized that the value of Q is the Mach number dependent, nondimensional heat release for *thermally choked flow*. Since the
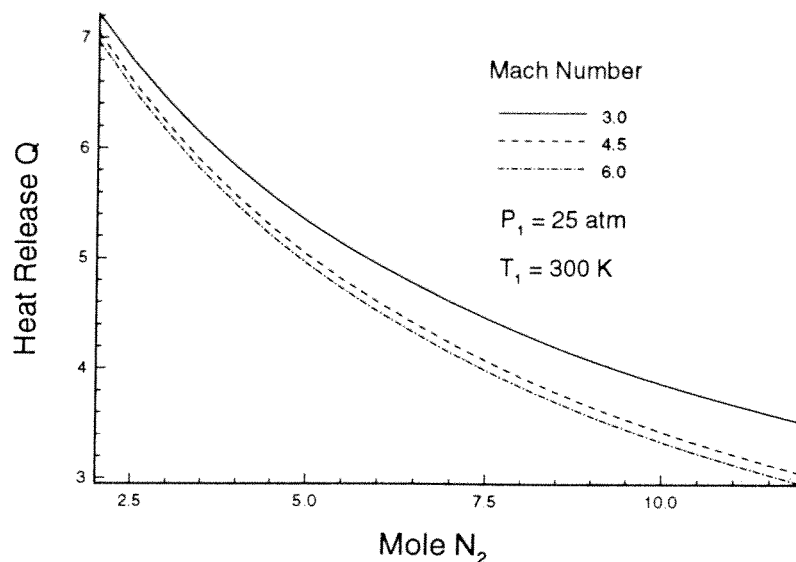
Fig. 3.3   Thermally choked heat release for a $2O_2$ +
$2.8CH_4$ + XN_2 class of mixture.

flow cannot be thermally choked in the full tube area behind the projectile in transdetonative and superdetonative operation while producing positive thrust, this value of Q is not the actual heat release.   It is, however, believed to be at least qualitatively indicative of the actual heat release and provides a self-consistent measure for comparing the effective heat release of different chemistries under similar flow conditions.   Even in experiments where the flow did not ignite, a value of Q is ascribed to the experiment *as if it were* achieving full chemical equilibrium and choking in the tube behind the projectile.

3.2 Experimental Configuration

The process by which the combustion wave is initiated and stabilized on the projectile is an extremely complicated and unsteady interaction between an obturator and projectile occurring upon impact with the first stage of ram accelerator propellant.[11] Since the purpose of these experiments is to determine the limits of ram accelerator operation, as opposed to starting, the experiments must be carefully isolated from the combustion initiation process. To achieve this, a starter stage of the standard propellent mixture described above ($2O_2$ + $2.8CH_4$ + $5.7N_2$) is used. This mixture can consistently initiate and stabilize a combustion process with the projectile. If the entire ram accelerator is filled with this mixture, it will accelerate a magnesium projectile from the entrance speed of 1100 m/sec to 1975 ± 25 m/sec, where an unstart occurs (see Fig. 2.9). Hence, this mixture forms the "control" in the experiments to follow.

It is believed that within the first meter of the ram accelerator test section the obturator and starting transients are gas dynamically decoupled from the projectile, leaving it in quasi-steady operation. In this series of experiments, the projectile was allowed to travel for a minimum of 2 m in this nominal mixture. The projectile then transitioned into the test mixture, which was a variation of the starter stage with either increased or decreased nitrogen dilution. These two stages were separated by a thin (0.5 mm) Mylar diaphragm. For experiments in which a high Mach number transition was desired, the starter stage was lengthened to provide a greater velocity gain before the transition. These experimental configurations are shown schematically in Fig. 3.4.

Investigation of
Low Mach Number Transition

Starter Stage   Test Stage

Investigation of
High Mach Number Transition

Starter/Accelerator Stage   Test Stage
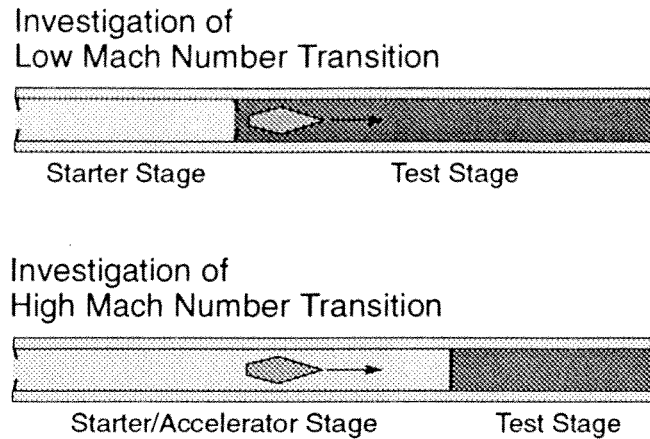
Fig. 3.4   Experimental   configurations   used   to investigate limits to the ram accelerator.

Although these experiments involved transitions into mixtures with significant changes in energetics and heat release, the sound speed never varied by more than 3%. Hence, there was no sudden shift in Mach number or acoustic impedance. In routine ram accelerator multistage operation, transitions are regularly made resulting in a nearly instantaneous change in Mach number from 4 to 3 (see Fig. 2.9(b)). Hence, the current experiments represent a relatively mild gas dynamic transition.

3.3 Experimental Procedure

The projectile was tracked down the length of the test section via electromagnetic probes until an unstart occurs, which could be determined unambiguously from pressure transducers mounted on the tube wall (see Fig. 2.10). The propellant fill pressure in all experiments (both starter and test stage) was 25 atm. After an experiment, samples of the propellant

mixture drawn from the ram accelerator tube immediately before firing were analyzed via gas chromatography to ensure the correct propellant mixture was used. Appendix A lists the results for analysis of the mixtures used in this experimental series. Although determining the absolute molar ratios to within 5% is difficult with the current gas analysis system, the molar ratios can be accurately varied in a relative and reproducible manner by increments as little at 2%, or about 0.2 mole of N_2 in a $2O_2 + 2.8CH_4 + XN_2$ class of mixture.

IV. Results

Three series of experiments were preformed. The initial experiments explored the limits to operation for a projectile entering the test mixture at Mach 3.8. The second series used a similar configuration, with the projectile now entering at Mach 4.2. Finally, in an attempt to determine the nature of the observed limits, projectiles were injected into the test mixture from an inert stage. The transition and final velocities of the projectiles are listed in Appendix A.

4.1 Low Mach Number Transition

The first series of experiments involved transition from the nominal, or starting stage, to the test mixture at a relatively low Mach number of 3.8. The projectile left the light gas gun with a velocity of 1130 ± 25 m/sec. After initiating combustion and accelerating the 2 m length of the starter stage, the projectile reached 1390 ± 20 m/sec at the transition to the test mixture. The remaining 14 m of ram accelerator were filled with the test mixture; although in only one experiment did the projectile continuously accelerate to the end of the test section. The results of these experiments, showing the projectile's velocity as a function of its position in the test section, are shown in Fig. 4.1. The velocity-distance profiles are actually higher order (4th-9th) polynomial curve fits to the first-order finite difference of the position-time history of the projectile as given by the electromagnetic probes. Note that the accelerations of the projectiles in the nominal starting stage were very similar, but upon
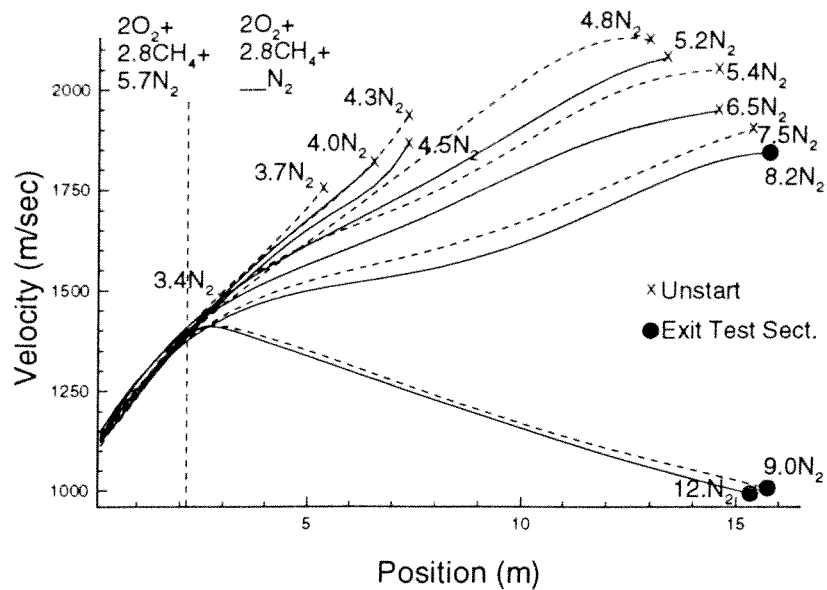
Fig. 4.1   Velocity-distance   data   for   Mach   3.8
transitions   into   variable   dilution
mixtures.

entrance to the test mixture, the performance varied greatly for the different
levels of N_2 dilution, with the more energetic propellants exhibiting higher
accelerations.   A detailed analysis of the performance of each propellant
mixture and comparison to the acceleration predicted by the "blackbox" model
of the ram accelerator will be presented in a future paper.   The primary
interest here remains on the gas dynamic phenomena that bound successful
operation.

For the two most dilute mixtures (9.0 and $12N_2$), the projectiles
actually decelerated. This concurs with the pressure profiles from the tube
wall transducers, which showed a clear wave fall-off ~0.5 m after transition
into the test mixture.   All the other mixtures exhibited at least some
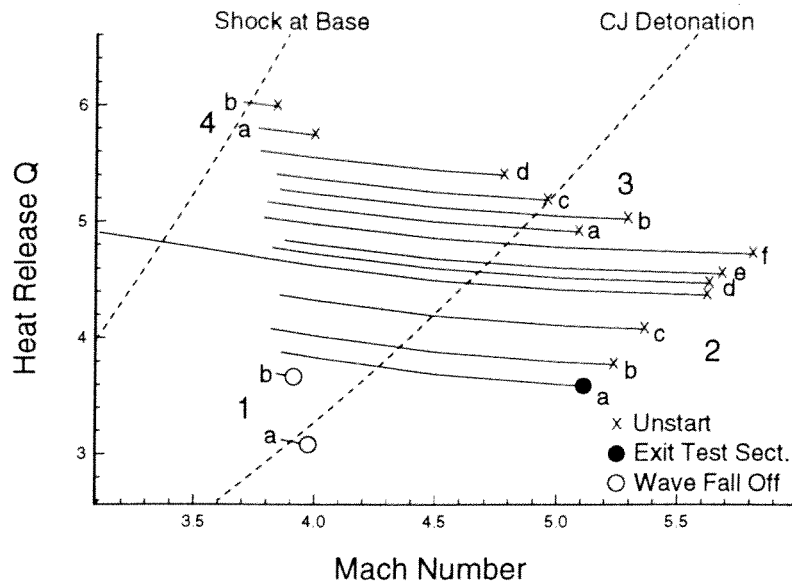
Fig. 4.2 Results of low Mach number transition experiments plotted as heat release vs. Mach number.

acceleration in the test mixture, except for the most energetic, which unstarted within ~0.5 m of the transition.

As a general rule, the less reactive/energetic a mixture, the farther the projectile drove into the test section before unstarting. The ultimate velocity, however, exhibited a maximum with respect to the amount of dilution. This observation becomes clearer when the data are plotted in the Q–M plane (Fig. 4.2), where examples of theoretical operational envelopes were shown earlier. The curve which begins at Mach 3.1 is the nominal, or starting, mixture. All experiments began on this curve and then transitioned, after 2 m of ram acceleration, to the appropriate test mixture, at which time the projectile is traveling at approximately Mach 3.8.

Experiment 2f in Fig. 4.2 (corresponding to a propellant of $2O_2$ + $2.8CH_4$ + $4.8N_2$) exhibited the maximum projectile velocity. Although the projectiles in the more heavily diluted mixtures unstarted at a lower Mach number, the reduced energetics of the mixture compromised the acceleration. Hence, the projectiles actually drove farther into the test section before failing. This longer history of heat transfer and projectile wear makes it difficult to ascribe these unstarts to pure gas dynamics. Indeed, it is known that projectiles constructed of different materials will drive farther and to higher final velocities in the nominal mixture,[12] suggesting an unstart mechanism which depends on a structural factor. For example, the projectiles may have sustained extreme fin erosion, leading to severe canting and eventual unstart,[13,14] or suffered melting and ablation due to aerodynamic heating.[15] Hence, the observed limit comprised of the unstarts 2a-f in Fig. 4.2 is *not* believed to be pure gas dynamic in nature, despite the fact that they form an envelope which is remarkably self-similar to the CJ detonation curve.

The more energetic mixtures plotted in Fig. 4.2, *i.e.* groups 3 and 4, unstarted earlier in the test section than the maximum velocity firing (2f). The fact that these projectiles unstarted earlier in the experiment, despite their reduced history of heat transfer and fin erosion, strongly suggests that the unstarts were gas dynamic in nature. As the mixture was made more energetic, these unstarts occurred at lower Mach numbers. For the most energetic of mixtures (group 4), the unstarts occurred almost immediately, *i.e.*, within the first meter, after transition into the test mixture. Hence, the group 3 and 4 unstarts appear to bound the maximum heat release for which the ram accelerator can operate in this class of mixture with this projectile configuration.

The extremely diluted mixtures (1a,b in Fig. 4.2) which exhibited combustion fall-off are also believed to be a pure gas dynamic limit to operation, since the fall-off occurred while the projectile retained structural integrity. It is interesting to note that the projectiles exhibited transdetonative performance until the mixture was diluted to a point where wave fall-off occurred.

Our earlier observation that the ram accelerator is not routinely operated in the region predicted by the one-dimensional, quasi-steady model of the flow field is borne out in these experiments. We see from Fig. 4.2 that almost all of the operation in these experiments occurred under conditions in which a normal shock would have fallen off the base of an ideal projectile or in which no thrust should be available at all, *i.e.*, in the transdetonative regime. Moreover, the observed "hot" limit appears to concur with the conditions under which a normal shock would just barely be supported on the projectile base.

4.2 High Mach Number Transition

The lack of an upper bound on heat release for the theoretical envelope in Fig. 2.4 suggests that the observed "hot" limit in these experiments may only apply when entering the mixture at Mach 3.8. Moreover, the device may be able to operate in more energetic mixtures via a higher Mach number transition. To answer this question, a second series of experiments was performed which used an additional 2 m of the nominal starting mixture before transition to the test mixture, as shown schematically in Fig. 3.4. The projectile now entered the test mixture at 1540 ± 25 m/sec or Mach 4.2. As
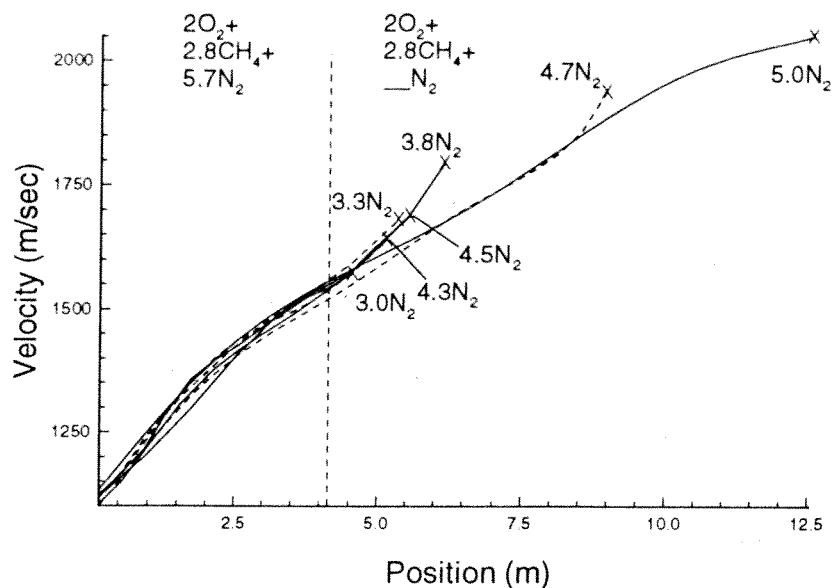
Fig. 4.3 Velocity-distance data for Mach 4.2 transitions into variable dilution mixtures.

mentioned previously, the longer projectile residence times in the test section required to observe an unstart in heavily diluted mixtures make the gas dynamic nature of these unstarts suspect. Hence, the emphasis in this second series is exclusively on the more energetic mixtures, for which the limits are believed to be purely gas dynamic in nature.

The results of these experiments are shown in Fig. 4.3. Again, the projectiles exhibit similar velocity profiles in the first stage of nominal propellant, then depart following entrance to the test stage. The well ordered sequence of unstarts as a function of mixture energetics observed in the previous section appears less distinct here. More dilute mixtures did not always drive the projectiles farther into the test section. The dependence of the Mach number range of operation on chemistry becomes clearer by again
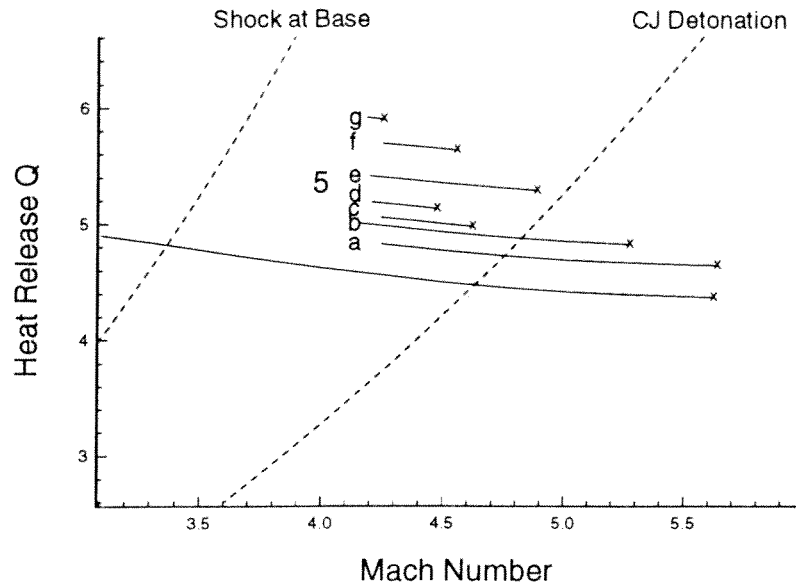
Fig. 4.4 Results of high Mach number transition
experiments plotted as heat release vs.
Mach number.

plotting the data in the Q–M plane. The Mach number of unstart did not

exhibit a monotonic decrease with decreasing dilution. Two of the group 5

experiments (c and d) failed at anomalously low Mach numbers. Although the

5c-d unstarts occurred ~1 m after transition, by which time the transition

transients are believed to have passed, this result leads to suspicions that

high Mach numbers may be less tolerant of transitions to more energetic

mixtures. For the most part, however, the observed operational limits appear

to concur with those found in the lower Mach number transition experiments.

The agreement in observed operational limits between the low and high Mach

number transition experiments reinforces the supposition that the limits are

pure gas dynamic in nature. The two experiments in which the projectiles

unstarted anomalously early, however, suggest that high Mach number

transitions might be more susceptible to transition induced failure, either due to unsteady flow phenomena, or the lengthened history of fin wear and heat transfer mentioned earlier.

4.3 Limits to Supersonic Coasting

While these experiments have succeeded in mapping out the operational envelope for this particular class of propellant and projectile configuration, they do little to reveal the nature of the limiting mechanism, the unstart. Consideration of the one-dimensional, quasi-steady model of the flow field indicates that there are two possible unstart mechanisms: premature combustion leading to a choking of the flow at the throat and the disgorging of the normal shock/combustion wave system due to excessive heat release behind the body. Ideally, the former mechanism (precombustion leading to choking at the throat) is independent of the combustion wave behind the projectile. If this is the relevant mechanism, it should result in an unstart upon entrance into the test mixture regardless of the presence of a combustion wave behind the projectile. The second unstart mechanism, pushing the normal shock over the body of the projectile, requires that a combustion wave first be initiated behind the projectile.

Of course, viscous flow effects tend to blur this distinction, since the flow field upstream of the shock system is no longer purely hyperbolic in nature, and combustion can be propagated upstream via the boundary layer. Nevertheless, we can attempt to differentiate these two by "stripping" the combustion wave from the projectile before it enters the test mixture. The thermally choked ram accelerator is believed to require the complicated and

Investigation of Supersonic Coast
at Low Mach Number

Starter Stage   Inert Stage   Test Stage
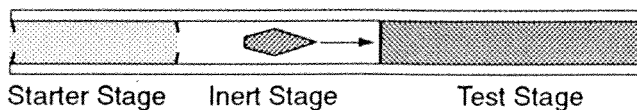
Investigation of Supersonic Coast
at High Mach Number

Starter/Accelerator Stage   Inert Stage   Test Stage
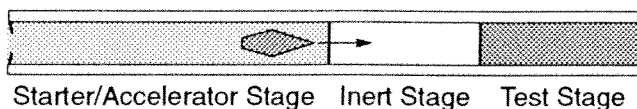
Fig. 4.5   Schematic of experiments to determine
limits to the projectile's ability to
supersonically coast through a mixture.

unsteady interaction with the obturator to initiate operation. Hence, by stripping the combustion wave before entering the test mixture, the projectile should "coast" supersonically through the test mixture, while it steadily decelerates. If the coasting projectile immediately unstarts, then the unstart mechanism is likely some form of precombustion leading to thermal choking at the projectile throat. On the other hand, if the projectile coasts uneventfully through a test mixture in which an accelerating projectile would unstart, the unstart mechanism requires the presence of a driving combustion wave.

The combustion strip is accomplished via a 4-m-long inert stage placed between the starter/accelerator stage and the test mixture. This inert mixture consists of a chemistry identical to the test mixture, only with the oxygen swapped for nitrogen. For example, if a test mixture of $2O_2 + 2.8CH_4 + 3N_2$ is used, the inert stage immediately upstream of the test section is $5N_2 + 2.8CH_4$. This is shown schematically in Fig. 4.5. Matching the gases in this
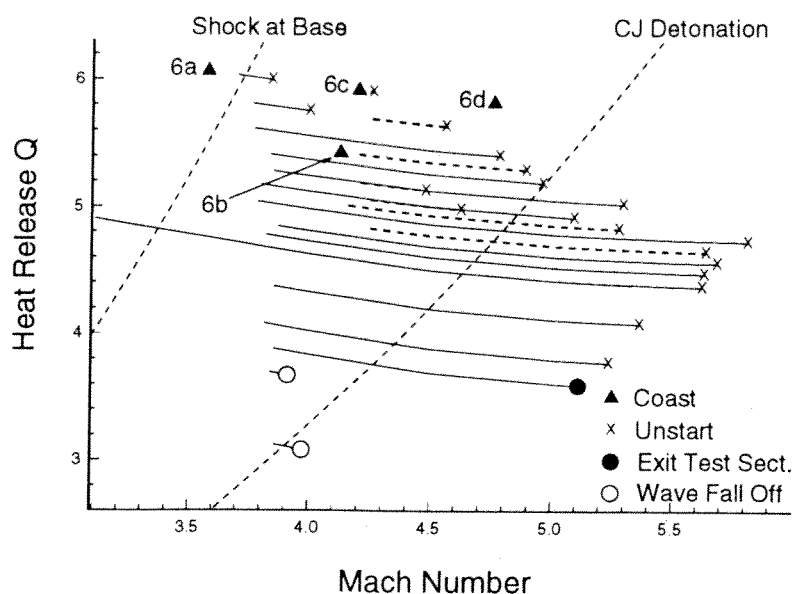
Fig. 4.6 Observed limits to ram accelerator operation. Triangles indicate successful projectile coasting. Dashed lines represent the high Mach number transitions (cf. Fig. 4.4).

way ensures the smoothest possible transition. This ability to strip off the combustion wave is a luxury available only with thermally choked operation, since the superdetonative modes of operation, which are capable of inducing combustion via shocks, are believed to be hyperbolic in nature.

Only four such experiments were performed, each near the observed "hot" limit determined in the prior experiments. The test mixtures used for these experiments were the most energetic of those used in these sets of experiments, e.g., $2O_2 + 2.8CH_4 + 3.0N_2$, which has a heat release parameter value of $Q \approx 6.0$. The results of these experiments are shown, along with the low and high Mach number transition results, in Fig. 4.6 (labeled 6a-d). In all

cases, a projectile entering the test mixture after passing through an inert stage was able to coast successfully in the combustible gas.

In the lowest Mach number transition case ($M=3.5$) into a mixture of $2O_2 + 2.8CH_4 + 3.0N_2$, the projectile was able to coast uneventfully through the entire 8 m length of the test section (see 6a in Fig. 4.6). The pressure traces showed no signs of combustion activity around the projectile or in the wake and were identical to a projectile coasting through the inert stripping stage. This contrasts with experiment 4b (see Fig. 4.2), where a projectile with the combustion wave already attached unstarted almost immediately upon transition into this same mixture at a similar velocity. It should be mentioned that no ram acceleration was required in this particular experiment; the light gas gun was sufficient to provide the necessary entrance velocity to the inert stage. The remaining combustion stripping experiments involved at least some ram acceleration, although the 4 m inert stripping stage should have eliminated any gas dynamic history effects.

The next experiment in this series involved a higher Mach number transition ($M = 4.2$) from the inert stage into a less energetic mixture ($2O_2 + 2.8CH_4 + 3.8N_2$). This mixture exhibited sustained acceleration in the prior high Mach number transition experiments. The pressure traces from this experiment are shown in Fig. 4.7, where the nominal probe spacing is 0.4 m. An outline of the projectile, scaled to the average velocity for this sequence, shows its relative size. Trace a and b in Fig. 4.7, from the inert, combustion stripping stage, exhibit a pressure profile typical of nonreacting flow. Upon entrance to the combustible mixture, pressure traces c through g show a distinct pressure pulse developing in the wake and eventually catching up with the projectile. The peak of this combustion wave travels with a velocity
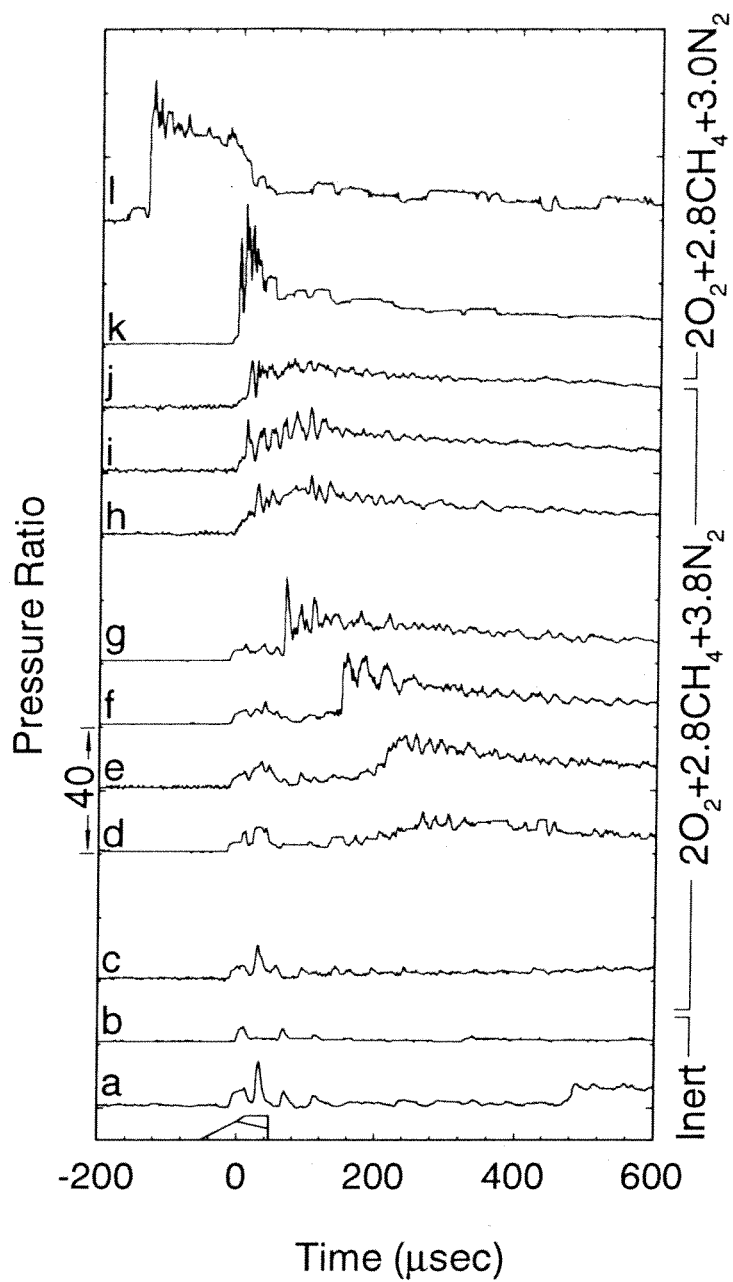
Fig. 4.7 Pressure traces from stripping and reignition of the driving combustion wave.
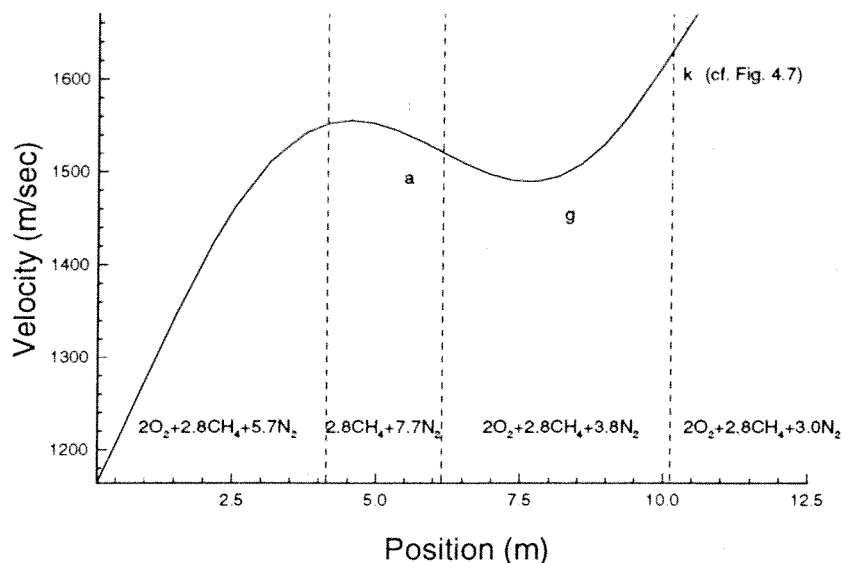
Fig. 4.8   Velocity-distance data for stripping and
reignition of the driving combustion wave.

of roughly 2 km/sec with respect to the stationary tube. Since the wake of a
supersonic projectile is relatively quiescent with a velocity of only a few
hundred m/sec with respect to the stationary tube,[16] this high propagation
velocity suggests a detonation or a deflagration to detonation transition. Note
that during this time the pressure profile at the projectile throat remains
unchanged in character and amplitude, which we would not expect if
significant heat release was occurring there. The normal shock residual from
the combustion stripping process (visible in trace *a* only) is ~1.5 m
downstream of the projectile by the time of traces *d-g* and hence is not
believed to be responsible for the re-ignition in the wake.

By pressure trace *h* in Fig. 4.7, this combustion wave is in direct
communication with the projectile, resulting in re-established projectile
acceleration, visible in the velocity-distance data plotted in Fig. 4.8.

Unfortunately, at this point the projectile transitioned into a new stage of a more energetic mixture ($2O_2$ + $2.8CH_4$ + $3.0N_2$) and promptly unstarted. The mechanism of this unstart is not certain, although it is likely that an unstart was imminent before transition, since the projectile velocity was approaching the gas dynamic limit of this mixture (Mach ~4.8) observed in the prior experiments. This additional staging was done in hopes of obtaining an economy of experiments, since the expectation was that the projectile would either coast uneventfully or promptly unstart. Hence, by using multiple stages of different mixtures, several data points could be collected in a single experiment. Since the projectile exhibited the ability to re-establish ram accelerator drive, this economy was not realizable and was abandoned in the remaining experiments.

A similar phenomenon was observed with a slightly higher entrance velocity (1550 m/sec or Mach 4.3) into the more energetic class of mixture ($2O_2$ + $2.8CH_4$ + $3.0N_2$), as seen in Fig. 4.9. Again, in transition from inert to reacting, no change in the throat pressure profile is visible. The projectile was able to coast for 2 m until the wake-initiate combustion wave overtook the projectile and unstarted. The unstart occurred in this case as soon at the combustion wave reached the projectile and no appreciable acceleration was observed. This is not surprising, since a projectile with the combustion wave already attached promptly unstarts upon entrance to this mixture. The fact that at a similar entrance velocity, a driving projectile unstarts almost immediately (< 0.5 m) upon transition while a projectile stripped of the combustion wave can coast for at least 2 m strongly suggests that the unstart mechanism in the observed "hot" limit requires the presence of the combustion

46
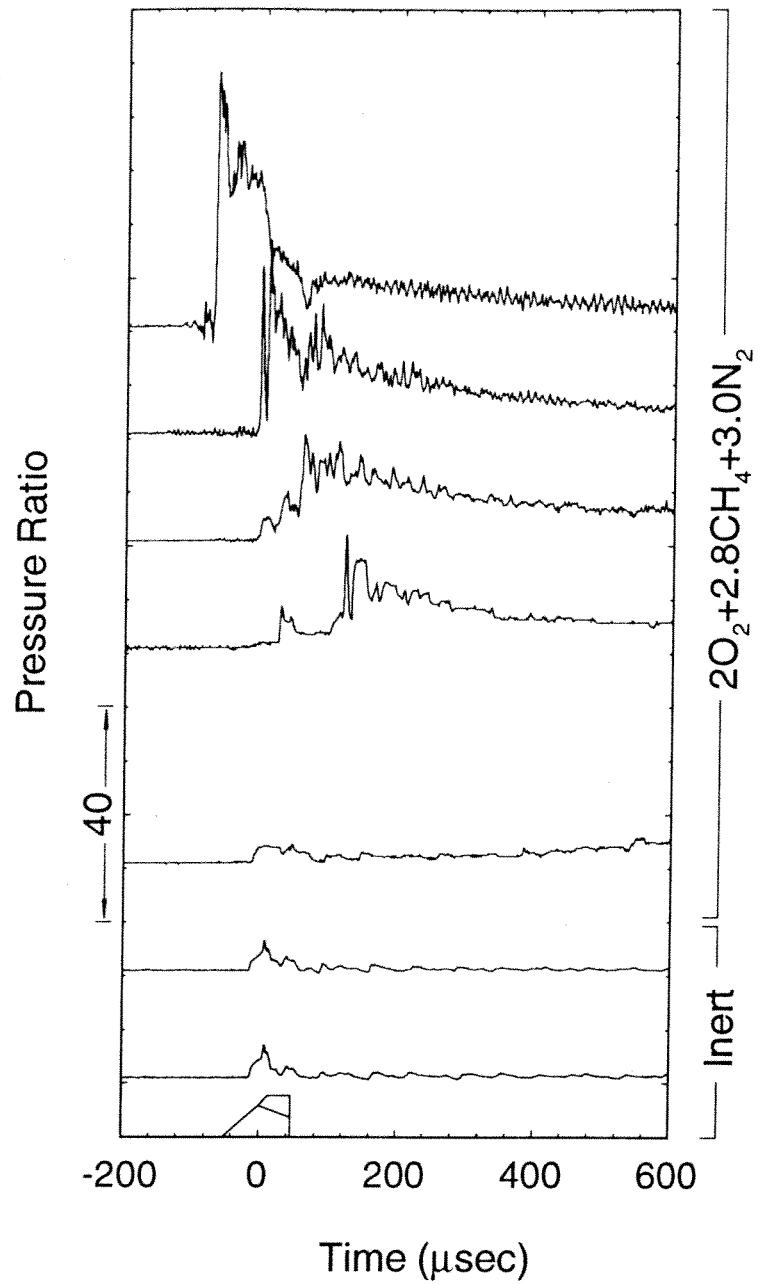
Fig. 4.9 Pressure traces from stripping and reignition of the driving combustion wave in a more energetic mixture.

wave behind the projectile and is *not* a simple choking of the flow due to shock-induced or boundary layer precombustion.

Nearly identical results were obtained with an even higher entrance velocity (1750 m/sec or Mach 4.8), as seen in Fig. 4.10. This velocity is beyond the observed velocity limit for these more energetic ($Q > 5.5$) mixtures. Hence, this experiment lies to the upper right of the observed envelope of operation (see 6d in Fig. 4.6). Again, the pressure profiles at the throat exhibit no signs of incipient unstart until the wake initiated combustion wave has overtaken the projectile, reinforcing the supposition that this unstart mechanism is not exclusively a phenomenon of the flow at the throat.

It should be noted that wake ignition phenomena have be observed in hypervelocity firings of spheres into hydrogen/oxygen and hydrogen/air mixtures.[16] In these experiments, detonation waves observed propagating up the wake of the projectile were believed to be generated by the muzzle blast of the initial launcher, although the possibility of self ignition at the end of an induction period after the projectile passed was mentioned. These combustion waves had a velocity inferior to the projectile. Experiments in which a wake-initiated wave overtook the projectile were noted by McVey and Toong, though no details were given.[17]

The ability of the ram accelerator to re-establish operation is an intriguing result. Not only does it elucidate the mechanism of unstart, it also suggests that interaction with the obturator may not be necessary to establish drive. Moreover, quasi-steady operation may be "forgiving" and reproducible under a variety of experimental initial conditions.

48
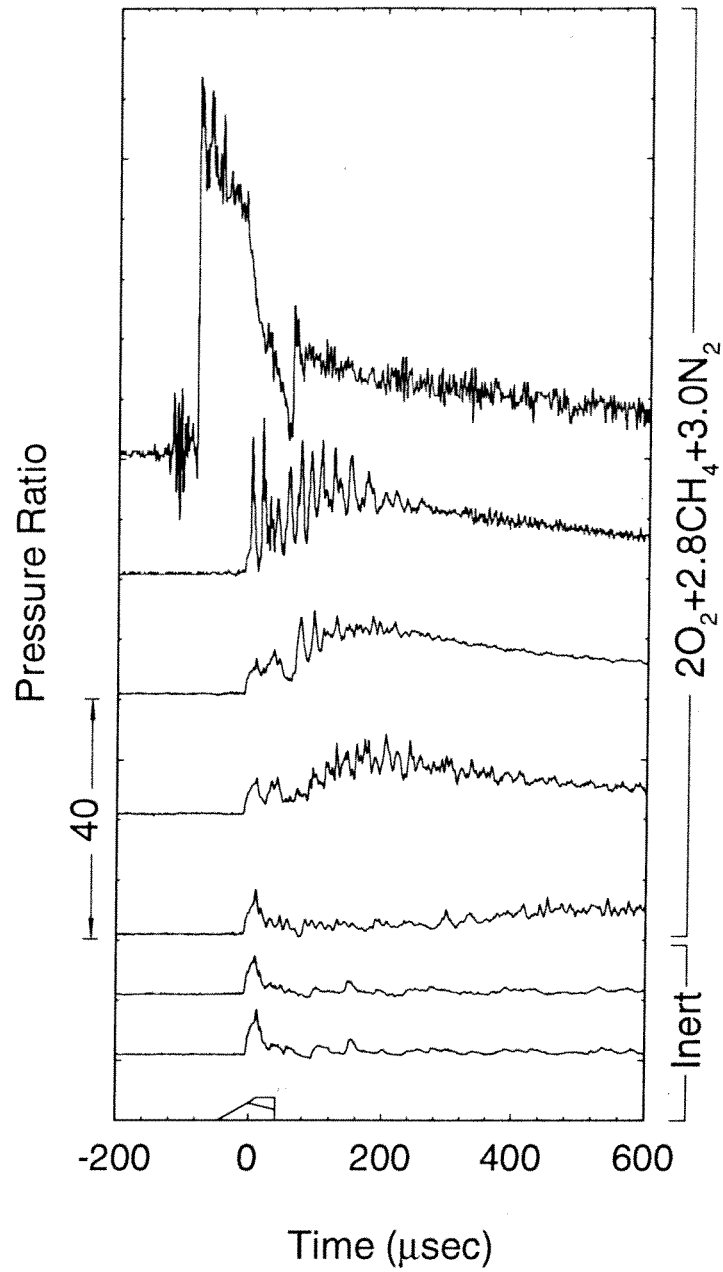
Fig. 4.10 Pressure traces from stripping and reignition of the driving combustion wave at higher velocity.

V. Analysis and Discussions

The experiments presented in the previous chapter identified four distinct limits to ram accelerator operation. These are shown, along with the experimental results, in a highly stylized fashion in Fig. 5.1. The line labeled "a" appears to bound the energetics of the mixture in which a projectile can successfully stabilize ram accelerator operation. Limit "b" is an observed maximum velocity which a projectile with the combustion wave already attached can achieve. The line "c" is not believed to be a gas dynamic limit, since the projectiles unstarted after relatively long residence times in the test section. Finally, "d" appears to bound the minimum mixture energetics required to stabilize the combustion wave on the projectile. These limits are,
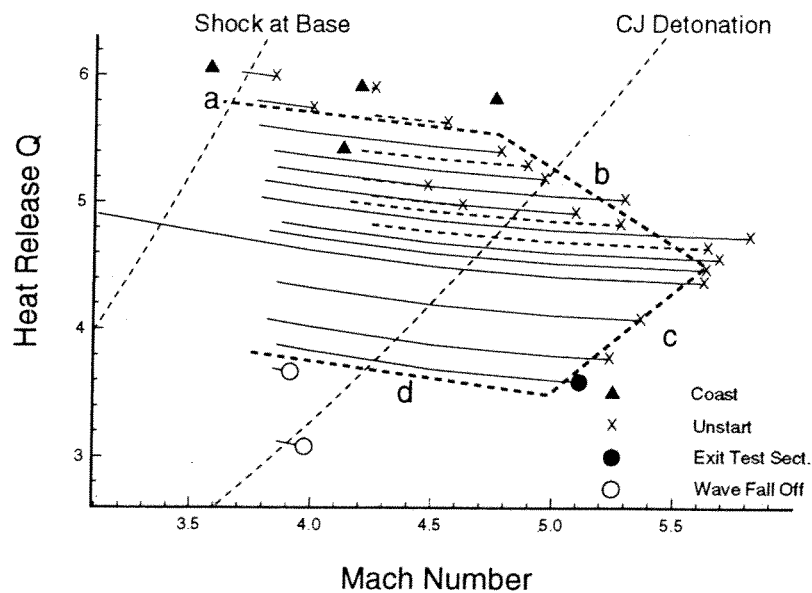
Fig. 5.1 Stylized representation of observed operational limits.

of course, dependent upon the parameters of the experiment and are drawn only as useful abstractions of the results in the previous chapter.

The limit on the heat release or energetics of the mixture (line "a" in Fig. 5.1) is not an unexpected result. A mixture which will not allow a combustion wave to stabilize on the projectile at all is bound to exist. The fact that this limit appears to coincide with the shock-at-base curve could be accounted for by the inadequacy of treating the complex shock system as a normal shock. The limit labeled "b" in Fig. 5.1 is more troubling. Although it lies near the CJ detonation limit, one must recall that the CJ curve is an ideal limit on thrust, *not* an unstart mechanism. As the projectile accelerates, it is moving further from both the sonic-at-throat and shock-at-throat unstart mechanisms in this Q–M plane. The conventional explanation, that a velocity limit exists for an accelerating projectile due to forebody combustion which will eventually unstart the projectile, does not apply here, as demonstrated by the successful coasting of projectiles at *above* the observed velocity limit in the most energetic of these mixtures. Moreover, in the context of our quasi-steady, one-dimensional model, it is difficult to envisage a mechanism which will force the once stable combustion wave system over an accelerating projectile.

Although this model has been criticized for treating the shock system, which is known to be complex, as a single normal shock, it is difficult to see how a more sophisticated modeling of the shock system would affect the qualitative nature of the results. Specifically, it is a well-known result that shock train end states are well predicted by the normal shock relations.[10,18] Moreover, a shock train responds to changing downstream boundary conditions (*i.e.*, back pressure) just as a normal shock does.[18,19] This conclusion makes the observed velocity limit all the more disturbing. Once a

projectile is started and the shock system is established, it should only recede with projectile acceleration, making an unstart less likely. Experimentally, just the opposite is observed: higher projectile velocities appear to drive the shock system past the throat, as was clearly observed in the combustion stripping/re-ignition experiments. This unknown mechanism forms the gas dynamic limit seen in Fig. 5.1 (line "b").

The conventional explanation is that as the projectile accelerates, increasing shock strengths and increasing total temperatures drive the kinetic rates to the point here heat release begins on the body. This heat release can couple with the shock system and drive the combined shock/combustion system closer to the throat and eventual unstart. This phenomenon was computationally simulated by Soetrisno et al.[20] What will be suggested here is an alternate explanation for this observed limit. This mechanism lies in a subtle distinction between ram accelerator gas dynamics and the conventional problem of stabilizing a normal shock in a diverging duct. This analysis relies heavily on experiments with shock trains in the isolator/combustor of scramjets performed by F. S. Billig and his associates at Johns Hopkins University Applied Physics Laboratory[19] and a recent interpretation of the role of the isolator advanced by Pratt and Heiser.[21]

5.1 Modeling of Shocks in Diverging Sections

Early research on supersonic combustion ramjets (scramjets) identified the importance of the distinction between the idealized normal shock wave and the observed, complex structure of a shock train,[19] or so called "pseudo-shock."[18] The presence of the shock train necessitates a constant area section

between the diffuser and the combustor called an isolator. The isolator is essential to prevent boundary layer separation, caused by the adverse pressure gradient associated with supersonic combustion unrelieved by area expansion, from propagating upstream and unstarting the inlet. The isolator also plays an important role in a dual mode scramjet operating in subsonic combustion mode, where the isolator must contain the shock train required to render the flow subsonic without the luxury of a physical throat to stabilize a normal shock.[21] The isolator and shock train, then, are the mechanism by which the scramjet adjusts the flow field supplied by the diffuser to the conditions demanded by the combustor. It was also realized early on in these efforts that the shock train structure could be reproduced and studied in overexpanded nozzle flow, with the throttled back pressure playing the role of the pressure demanded by the combustor.[19] Hence, the overexpanded nozzle forms the basis of work on shock trains in scramjets and will be our starting point here.

The ideal pressure profiles in a converging-diverging nozzle for a varying back pressure are shown in Fig. 5.2. For pressures greater than p_I, the subsonic solution dominates throughout the domain, and the flow is entirely isentropic. For a back pressure of p_{II}, the exit plane flow is perfectly matched to the back pressure, and again the flow is isentropic. For back pressures between p_I and p_{II}, the nozzle flow is said to be overexpanded and must adjust to the back pressure by some nonisentropic mechanism. For back pressures above p_{III}, this adjustment can be accomplished via a normal shock. Below this value, the flow is brought to the prescribed back pressure by an oblique shock, since a normal shock would yield too great a pressure increase, and is outside the assumptions of a one-dimensional model. Back pressures
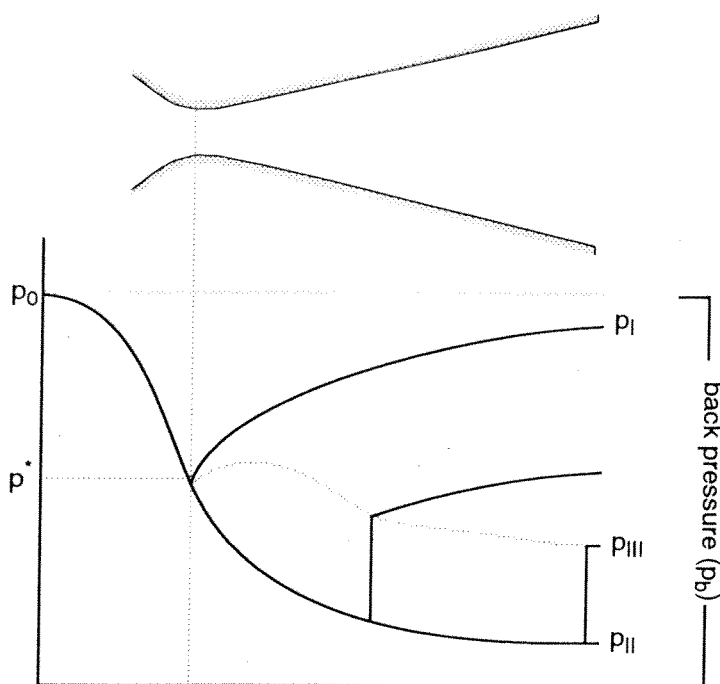
Fig. 5.2 Pressure distributions in an ideal converging-diverging nozzle.

below p_{II} yield an underexpanded nozzle, which compensates the flow with expansion fans outside the nozzle. This case is of little interest to us here; our emphasis remains on the overexpanded case.

Viscous considerations, such as boundary layers, considerably complicate the simple, one-dimensional flow field regimes outlined above. Beginning at the correctly expanded nozzle with back pressure p_{II}, modest increases in the back pressure can be compensated for by an oblique shock attached to the nozzle lip, as seen in Fig. 5.3(b). This oblique shock, however, creates an adverse pressure gradient which the boundary layer must traverse. The boundary layer can only withstand this adverse pressure gradient to a point, beyond which the flow will separate and the oblique shock will move

(a)   M < 1   M > 1   — expansion waves $p_b < p_{II}$

(b)   M < 1   M > 1   — shock wave $p_{II} < p_b < p_{II}r_{max}$

(c)   M < 1   M > 1 $p_{II}r_{max} < p_b = p_s r_{max}$

p_s

$p_b' < p_b$

(d)   M < 1   M > 1   M < 1 $p_{b(c)} < p_b < p_I$

(e)   M < 1   M > 1   M < 1 $p_{b(d)} < p_b < p_I$
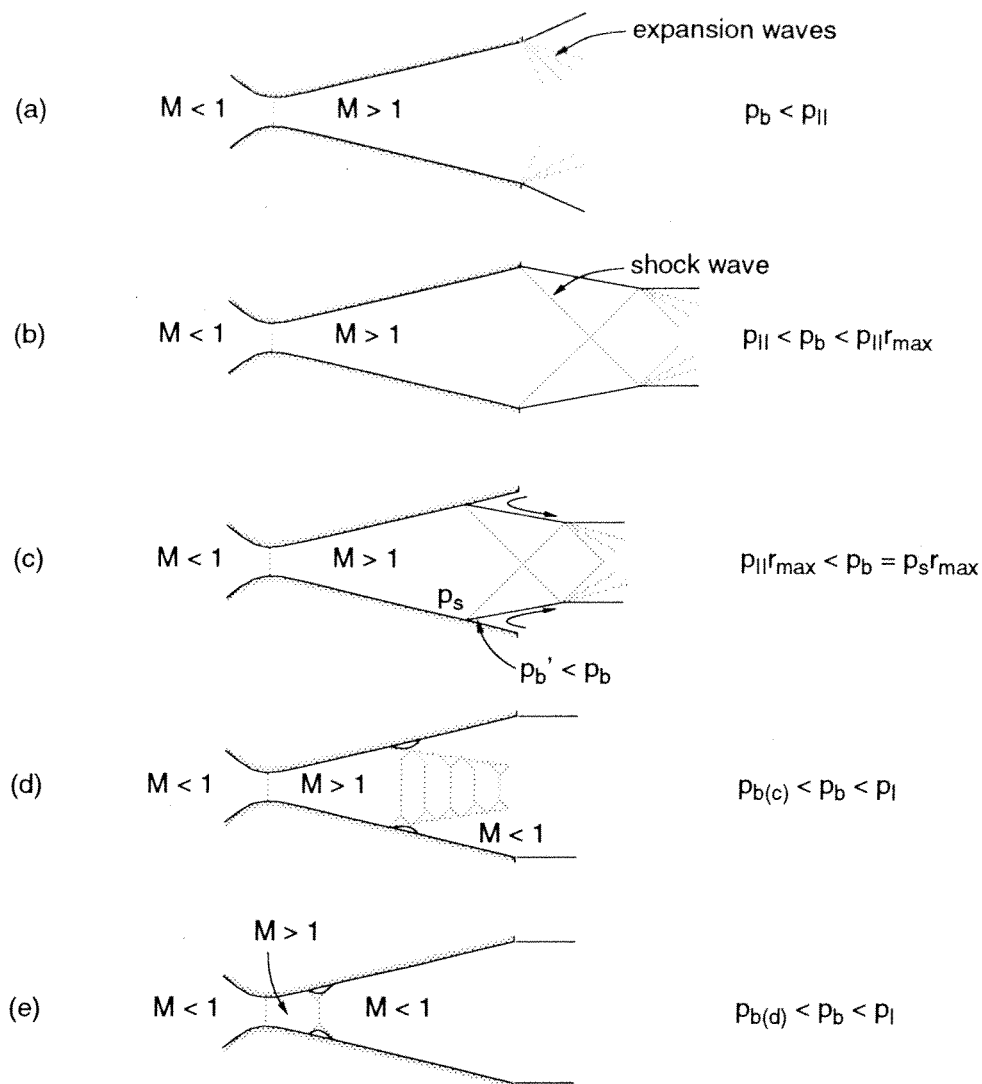
Fig. 5.3   Schematics   of   flow   fields   in   a   real
converging-diverging nozzle.[18]

upstream, as shown in Fig. 5.3(c).[18] The critical pressure ratio at which this
occurs will be called r_{max} ($r_{max} = p_b/p_{exit}$) and has a value usually cited at
approximately 2.5. The separation point and accompanying oblique shock will
proceed upstream to a position where the static pressure is sufficiently high to
match the back pressure after passing through an oblique shock with the

critical pressure ratio. The pressure in the separated region downstream of the oblique shock is actually somewhat less than the back pressure, since some fluid will be entrained between the jet and the walls, giving a critical ratio of $r_{max} = p_b'/p_s$, as seen in Fig. 5.3(c). The modifications to the qualitative results, however, should be slight.[18] If the back pressure is sufficiently high, the separation induced shock structure may develop into a complete shock train or pseudo-shock, with subsonic flow filling the exit plane and flow re-attachment. The flow now becomes directly analogous to the idealized one-dimensional analysis with a normal shock, only now the normal shock is replace by a finite length shock train (Fig. 5.3(d)). As the back pressure continues to increase, the shock train proceeds farther upstream where its reduced strength and the thinning boundary layers make it more closely resemble a single normal shock, shown in Fig. 5.3(e). These flow regimes in a real nozzle are directly analogous to the idealized, one-dimensional, inviscid problem, with the exception of the flow separation case (c) in Fig. 5.3. This separation shock, however, behaves phenomenologically similar to the ideal normal shock: it recedes further downstream with decreasing back pressure, *i.e.*, a decreasing adverse pressure gradient. Here, however, lies the subtle distinction between ram accelerator gas dynamics and the conventional converging-diverging nozzle. In the ram accelerator, the position of the normal shock is not governed by independently varying the back pressure, but instead by a varying initial total pressure, p_{o1}, and accompanying downstream pressure as dictated by the requirements of thermal choking.

5.2 Shock Structures in the Ram Accelerator

Unlike the conventional converging-diverging nozzle problem, where the upstream conditions remain unchanged and only the downstream pressure is varied, the ram accelerator has both upstream and downstream conditions varying simultaneously. Since the bulk of experimental data is for conditions under which a normal shock cannot be supported on the projectile, it is unlikely that a *complete* shock train or pseudo-shock can be supported on the body, especially since shock trains are usually 5 to 15 duct diameters in length.[18] Hence, the flow condition in Fig. 5.3(c) is likely to prevail in nominal ram accelerator operation, that is, flow separation with the separated region in direct contact with the back pressure. To determine how significant this separation may be, we must examine the back pressures demanded by the combustion wave.

For the purposes of this discussion, we will assume categorically that the flow is always thermally choked in the full tube area behind the projectile. Since the observed limit which is the subject of this discussion (line "b" in Fig. 5.1) is near the CJ detonation speed, this is not too limiting an assumption. We will also assume all the heat addition occurs downstream of the projectile. The static pressure and total pressure at the plane of thermal choking are uniquely determined by the condition of thermal choking in the full tube area. We can also compute that conditions at station 5 *without*

reference to the flow around the projectile (provided it is choking from the subsonic branch) via Shapiro's "useful integral relations":[10]

$$\frac{p_5}{p_6} = \frac{1}{M_5}\sqrt{\frac{1 + \frac{\gamma - 1}{2}}{1 + \frac{\gamma - 1}{2}M_5^2}} \cdot \frac{1}{\sqrt{\frac{Q}{\sqrt{1 + \frac{\gamma - 1}{2}M_1^2}} + 1}}$$

and the relation for simple T_0-change in a constant area duct:

$$\frac{p_5}{p_6} = \frac{1 + \gamma}{1 + \gamma M_5^2}$$

Solving this coupled set of equations will yield the pressure and Mach number at station 5.

We can also compute the pressure at the throat of the projectile, p_2, by assuming the flow to be isentropic over the forebody. The computed pressures at stations 2, 5, and 6 are compared to experiment in Ref. 9 and are found to be in sufficient agreement for the purposes of this qualitative calculation.

The static and total pressures (normalized by fill pressure, p_1) are plotted in Fig. 5.4 as a function of projectile Mach number for a Q value of 5. In all these calculations, we have assumed a constant γ of 1.4, again treating the flow as an inert working fluid with external heat addition between stations 5 and 6. Notice that the static pressure at the throat actually *decreases* with increasing projectile Mach number. Although the stagnation pressure p_{01} is dramatically increasing with projectile acceleration, the Mach number at the throat is also increasing, reducing the fraction of the total
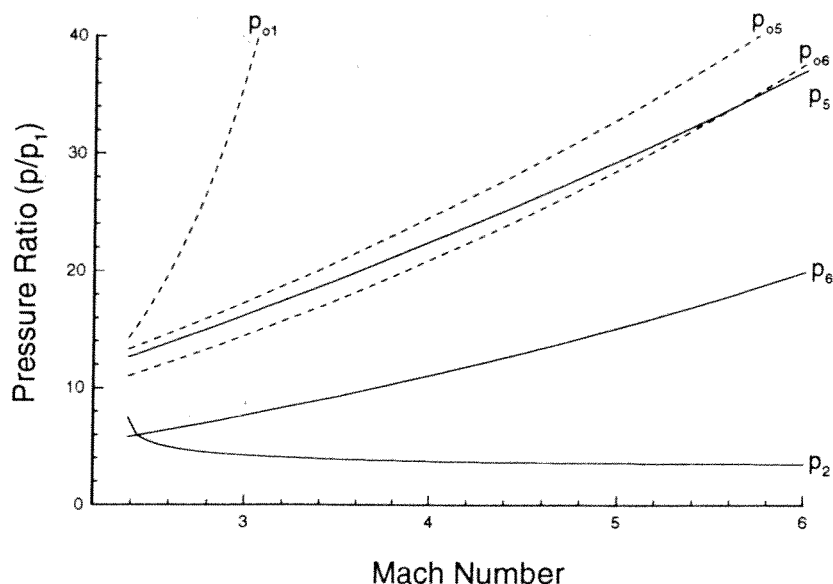
Fig. 5.4   Static and total pressures as predicted by
a one-dimensional flow field model.

pressure recovered there. The static and total temperatures at station 5 (the projectile base) and station 6 (the plane of thermal choking) show a pronounced increase with increasing projectile Mach number. Which of these pressures we should use for the "back pressure" to determine the extent of flow separation is open to interpretation. The case could be argued that the total pressures are appropriate, since the flow in the annular area around the projectile is exhausting to the *stagnated* flow in the wake of the projectile base. Alternatively, the separated flow there is in direct communication with the static pressure, either p_5 at the base or p_6 at the thermal choking plane. Regardless of which is the appropriate back pressure, the qualitative conclusion is the same: the back pressure is dramatically increasing with projectile acceleration while the throat pressure is remaining relatively constant. While ideal, one-dimensional calculations require a normal shock to

continuously recede with projectile acceleration, these pressure trends strongly suggest that the adverse pressure gradient, and hence flow separation, *becomes more significant with increasing projectile Mach number.* This is in sharp contrast to the conventional converging-diverging nozzle problem considered above, where the normal shock recedes due to a decreasing back pressure, which also causes any flow separation to recede as well.

To estimate how significant the flow separation might be, we will need to select one of the pressures plotted in Fig. 5.4 as the back pressure. For these calculations, we will select p_6, since it is a *thermodynamic* property of the choked flow and agrees well with the experimentally observed pressure at the choking plane.[9] Moreover, since the thermal choking is providing the equivalent to the throttling of the back pressure in the conventional converging-diverging nozzle problem, p_6 is perhaps the more consistent choice for the back pressure. Again, this selection should not affect the qualitative nature of the results, since all these pressures at stations 5 and 6 exhibit similar trends and are indicative of the pressure "demanded" by a thermally choked flow.

Finally, we must select a model for r_{max}, the critical pressure ratio for separation. The value of 2.5 appears accepted in the nozzle literature and is often cited (without reference) in contemporary texts on gas dynamics[22] and rocket propulsion.[23] This value seems to have its origins in experiments performed with overexpanded nozzles in the early 1950's by Summerfield *et al.*[24] Instead, we will select a theoretical model developed by Crocco for flow separation of turbulent boundary layers by interaction with an oblique shock on a flat plate without pre-existing pressure gradients.[25] The pressure ratio
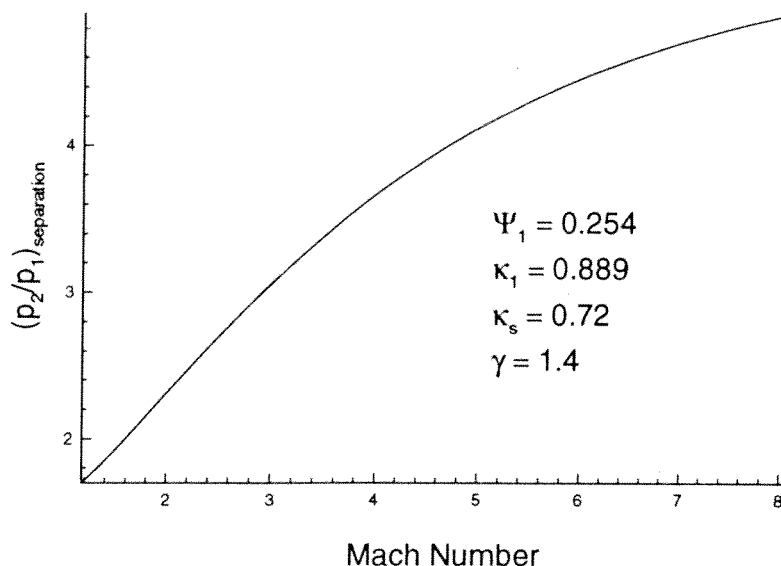
Fig. 5.5   Critical pressure ratio for separation by
an oblique shock wave.[25]

required to separate the boundary layer as a function of Mach number as
predicted by this model is shown in Fig. 5.5; values of velocity and velocity
distribution parameters used to generate this curve are shown in the figure.
This theory is particularly convenient in that it is Reynolds number and
boundary layer thickness independent. This model is in excellent agreement
with the experimental results of Bogdonoff and co-workers for oblique shocks
incident on turbulent boundary layers for a flat plate[26] and shows good
correspondence with the value for r_{max} of 2.5 cited above for the Mach
numbers (Mach 2 to 3) involved in experiments with overexpanded nozzles.

5.3 Theoretical Limits to Operation Revisited

With a model for flow separation, the conditions under which separation occurs can be easily estimated. Flow separation is not assumed to be detrimental until it reaches the projectile throat, where it can propagate into the diffuser and result in an unstart. Hence, by *assuming* the pressure at the throat to be at the critical ratio to the back pressure p_6, the onset of throat separation can be directly computed in terms of the projectile Mach number and the heat release parameter Q. This relation can be plotted directly in the Q–M plane, where the previous theoretical and experimental limits to operation were displayed, as seen in Fig. 5.6. Since the base, or back, pressure increases with projectile Mach number while the throat pressure is relatively constant, the separation-at-throat criterion imposes a *maximum*
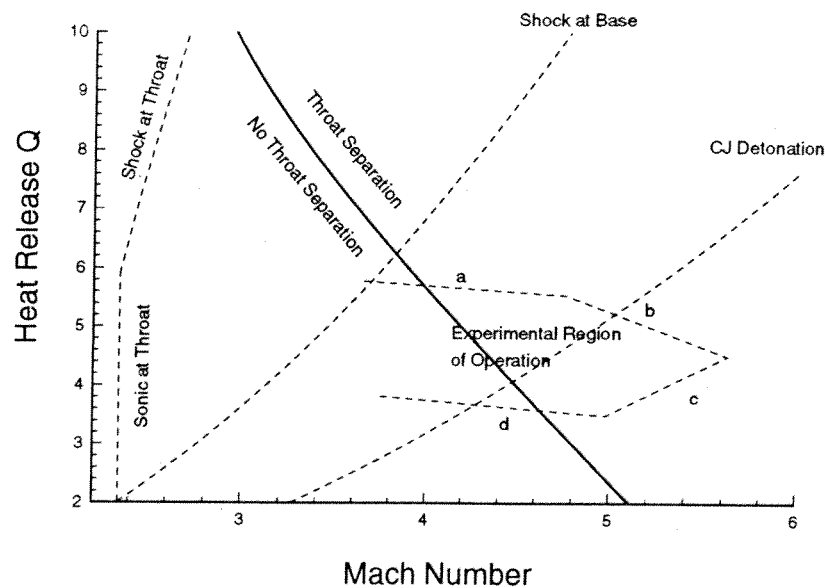
Fig. 5.6 Onset of flow separation at the throat compared to experimental and theoretical envelopes.

velocity limit, in contrast to the previous unstart mechanisms (shock-at-throat, sonic-at-throat), which were *minimum* velocities required for operation. More energetic mixtures (higher Q) have higher back pressures (at both station 5 and 6) while the throat pressure is unaffected by the heat release. Hence, the separation limit is reached at lower Mach numbers in the "hotter" mixtures. This trend is exactly what was observed in the experimental results of the previous chapter: a maximum velocity, which becomes lower with increasing heat release, beyond which the projectile will unstart.

Although this model predicts flow separation occurring at the projectile throat for about half the operational envelope, this relation can probably be brought into better agreement with the observed limits by incorporating a nonisentropic model of the diffuser and an improved value for the effective back pressure. The important point remains that this relation qualitatively captures an observed velocity limit, and in comparison to limit "b" has a remarkably similar slope. This similarity in trends suggests that shock induced separation phenomena could be significant and warrant further investigation.

With these results in mind, it is interesting to review the CFD results of Soetrisno *et al.*[13,20,27] Early simulations of ram accelerator flowfields with the Euler (inviscid) equations were unable to capture transdetonative phenomena and showed the shock system monotonically receding with projectile acceleration.[27] A full Navier-Stokes simulation, however, shows the shock/combustion system moving back up the projectile body as the projectile approaches the CJ detonation speed, resulting in the characteristic increase in projectile acceleration.[20] The explanation provided was that boundary

layer combustion allowed the shock/combustion system to propagate upstream.[20] The considerations of this chapter suggest a possible different mechanism: increasing boundary layer separation as a result of higher downstream combustion pressures.

In reality, this distinction between boundary layer precombustion and "postcombustion" induced boundary layer separation is artificial. These two phenomena are likely to be intimately coupled. Nowhere is this more dramatically demonstrated than in the expansion tube experiments of Srulijes *et al.*[28] In these experiments, a blunt, forward facing, vertical fin subjected to superdetonative flow is able to influence the supersonic flow at an upstream distance several times the fin's height via combustion in a separated boundary layer. The upstream influence is not present when an inert gas is used, proving that combustion is the mechanism of this upstream propagation. Obviously, shock wave, boundary layer, and combustion mutual interactions are important enough phenomena in ram accelerator gas dynamics to necessitate full Navier-Stokes, as opposed to inviscid, simulations.

VI. Recommendations and Conclusions

The operational envelope for an oxygen/methane/nitrogen based propellant mixture with a fuel equivalence ratio of 2.8 has been investigated. By varying the diluent concentration, limiting phenomena were observed from immediate unstart to combustion wave fall-off. The regimes of chemistry in which the projectile can operate form a well defined envelope in the heat release-Mach number $(Q-M)$ plane. Of course, these conclusions apply only to a single class of propellant mixture at a particular fill pressure for the projectile geometries used. It is with this caveat, *i.e.*, that the results obtained here can only be applied with confidence to experiments with similar parameters, that the potential for future work lies. Whether these results are universal phenomena to be encountered in all implementations of the ram accelerator could be answered, in part, by an experimental series outlined below.

6.1 Recommendations for Future Work

All of the theoretical analyses presented here treated combustion phenomena as equilibrium properties occurring at well defined, although arbitrarily prescribed, locations. No attention was given to finite rate chemistry considerations, with gas dynamics being treated as the first order effect. While any theoretical prediction of the influence of finite rate chemistry would likely require sophisticated computational modeling, the observed effects could possibly be gleaned from minor modifications to the

experimental series presented in Chapter 4. Higher propellant fill pressures, for example, should drive the kinetic rates up, exaggerating any precombustion effects. If the operational envelope is significantly reduced, then kinetic rates likely play an important role. On the other hand, an operational envelope unaffected by higher fill pressures suggests that equilibrium properties, which are relatively pressure insensitive, are the dominate factors, as was the assumption here. Varying the fill pressure, however, also changes the Reynolds number, raising the specter of viscous effects. Other possibilities include varying the fuel equivalence ratio instead of the dilution, or varying both. Again, the theoretical envelope in the Q–M plane is independent of the chemistry used, while the kinetic rates are certainly not.

Not only is the means by which the chemistry is varied, but the choice of the mixture itself is an area for further study. Fuel/oxidizer mixtures diluted with argon or carbon dioxide, with attendant lower acoustic speeds and detonation velocities, would allow a more complete exploration of the operational envelope, especially at higher Mach numbers. Projectiles accelerated to the desired test velocity via more conventional mixtures, while still retraining structural integrity, would experience "pure" gas dynamic phenomena at high Mach numbers, as opposed to the coupled gas dynamic/ structural phenomena believed to have been observed in the high Mach number unstarts in this series.

Variations in projectile geometry are another obvious continuation to these experiments. The theoretical analysis presented here suggests that the throat-to-tube area ratio is the critical geometric parameter. The fact that the projectile can successfully coast through a mixture in which a driving

projectile would immediately unstart suggests that more energetic mixtures may be accessible through a reduced annular throat area, as was argued in Section 2.2. The suggestion in Chapter 5 that this unstart mechanism may be a separation-induced oblique shock rather than a normal shock being forced past the throat does not alter this conclusion; a reduced throat simply increases the downstream back pressure, and hence the Mach number and energetics of the mixture, required to force the separation point into the diffuser. Alternatively, a series of experiments wherein the throat area is varied may help to further elucidate the unstart mechanism.

Finally, the intriguing ability of a projectile, stripped of the combustion wave, to re-establish ram accelerator drive warrants a more detailed look. Not only could further experiments of this class improve an understanding of unstarts, especially at higher Mach numbers, the results also have implications to the fundamentals of how the combustion process is able to be stabilized at all.

It is hoped that any such investigations can be performed with sufficient resolution to identify unmistakable trends, as was the case in the experiments presented here. Such trends are not only essential to the assessment of any theory or model, but are also the first steps toward an optimized, high performance ram accelerator.

6.2 Conclusions

In varying the mixture energetics, distinct limits to ram accelerator operation have been identified. A relatively wide range of chemistry ($3.8 < Q < 5$) continuously accelerates the projectile through the CJ detonation speed and

into the superdetonative regime, where the unstart mechanism is believed to depend on the projectile's structural integrity. Operation at Mach numbers above which one-dimensional theory predicts the normal shock can be stabilized on the body indicates that this model is inadequate for predicting the observed operational limits. The one-dimensional model also fails to account for an observed upper limit ($Q \approx 6$) on the energetics of the mixture. This limiting mechanism requires the presence of a combustion wave behind the projectile, since projectiles exhibit the ability to coast through, and even re-establish operation in, the mixtures which form this "hot" limit.

The failure of the one-dimensional model to predict the observed limits motivated an investigation of flow separation induced by high combustion pressures. Implementation of a simple separation model, based on previous analysis of overexpanded flows in supersonic nozzles, produced a new theoretical limit to operation which captures much of the experimentally observed phenomena. It is more likely, however, that coupled, boundary layer/ shock/combustion interactions are responsible for the observed limits to the ram accelerator. These experimental results and theoretical considerations are indicative of the range of phenomena that must be addressed by analytical and computational flow field models to accurately predict the operational characteristics of the ram accelerator.

In conclusion, the state of ram accelerator theory is incomplete. The development in many ways parallels the progress of detonation theory. The modified Hugoniot, or "blackbox," analysis of the ram accelerator accurately predicts the thrust of the thermally choked mode, just as the Chapman-Jouguet relations give the velocity of a detonation wave. Neither approach yields any information about the stability of the process, since both ignore the

internal details. The simple, one-dimensional model of a detonation wave (the ZND model) is similar to the model of the flow field presented in Chapter 2. While the ZND model of a detonation wave is inherently unstable since it fails to account for the complex structure of the detonation front, the one-dimensional model of the ram accelerator fails to define an envelope of operation that agrees with the experimentally observed limits. Unlike detonation theory, however, the missing component, or components, to ram accelerator theory have yet to be unambiguously identified.

References

1.   Hertzberg, A., Bruckner, A.P., and Bogdanoff, D.W., "Ram Accelerator: A New Chemical Method for Accelerating Projectiles to Ultrahigh Velocities," *AIAA Journal*, Vol. 26, No. 2, 1988, pp. 195-203.

2.   Bogdanoff, D.W., "Ram Accelerator Direct Space Launch System: New Concepts," *Journal of Propulsion and Power*, Vol. 8, No. 2, 1992, pp. 481-490.

3.   Bruckner, A.P., Knowlen, C., and Hertzberg, A., "Applications of the Ram Accelerator to Hypervelocity Aerothermodynamic Testing," AIAA Paper 92-3249, July 1992.

4.   Kruczynski, D., "Experimental Demonstration of a 120 mm Ram Accelerator," 29th JANNAF Combustion Subcommittee Meeting, NASA Langley Research Center, Hampton, VA, October 19-23, 1992.

5.   Giraud, M., Legendre, J.F., and Simon, G., "Ram Accelerator Studies in 90 mm Caliber," 43rd Meeting of the Aeroballistic Range Association, Columbus, OH, September 28-October 2, 1992.

6.   Hertzberg, A., Bruckner, A.P., and Knowlen, C., "Experimental Investigation of Ram Accelerator Propulsion Modes," *Shock Waves*, Vol. 1, 1991, pp. 17-25.

7.   Bruckner, A.P., Knowlen, C., Hertzberg, A., and Bogdanoff, D.W., "Operational Characteristics of the Thermally Choked Ram Accelerator," *Journal of Propulsion and Power*, Vol. 7, No. 5, 1991, pp. 828-836.

8.   Knowlen, C. and Bruckner, A.P., "A Hugoniot Analysis of the Ram Accelerator," *Shock Waves*, edited by K. Takayama, Springer-Verlag, Berlin, 1992, pp. 617-622.

9.   Knowlen, C., "Theoretical and Experimental Investigation of the Thermodynamics of the Thermally Choked Ram Accelerator," Ph.D. Dissertation, University of Washington, April, 1991.

10. Shapiro, A.H., *The Dynamics and Thermodynamics of Compressible Fluid Flow*, Vol. I, John Wiley and Sons, NY, 1953, Chs. 5, 7, 8.

11. Burnham, E.A., Hinkey, J.B., and Bruckner, A.P., "Investigation of Starting Transients in the Thermally Choked Ram Accelerator," 29th JANNAF Combustion Subcommittee Meeting, NASA Langley Research Center, Hampton, VA, October 19-23, 1992.

12. Auzias de Turenne, J., "An Analysis of Ram Accelerator Projectile Materials," AIAA Paper 92-0262, January 1992.

13. Soetrisno, M., Imlay, S.T., and Roberts, D.W., "Numerical Simulations of the Superdetonative Ram Accelerator Combusting Flow Field," AIAA Paper 93-2185, June 1993.

14. Hinkey, J.B., Burnham, E.A., and Bruckner, A.P., "Investigation of Ram Accelerator Flow Fields Induced by Canted Projectiles," AIAA Paper 93-2186, June 1993.

15. Naumann, K.W., "Heating and Ablation of Projectiles During Acceleration in a Ram Accelerator Tube," AIAA Paper 93-2184, June, 1993.

16. Behrens, H., Struth, W., and Wecken, F., "Studies of Hypervelocity Firings into Mixtures of Hydrogen with Air or with Oxygen," *Proceedings of the Tenth Symposium (International) on Combustion*, The Combustion Institute, 1965, pp. 245-252.

17. McVey, J.B., and Toong, T.Y., "Mechanism of Instabilities of Exothermic Hypersonic Blunt-Body Flows," *Combustion Science and Technology*, Vol. 3, 1971, pp. 63-76.

18. Crocco, L., "One-Dimensional Treatment of Steady Gas Dynamics," in *Fundamental of Gas Dynamics*, H.W. Emmons, Ed., Volume III of *High Speed Aerodynamics and Jet Propulsion*, Princeton University Press, Princeton, NJ, 1958, pp. 115-130, 166-171.

19. Billig, F.S., "Research on Supersonic Combustion," *Journal of Propulsion and Power*, Vol. 9, No. 4, 1993, pp. 499-514.

20. Soetrisno, M., Imlay, S.T., and Roberts, D.W., "Numerical Simulations of the Transdetonative Ram Accelerator Combusting Flow Field on a Parallel Computer," AIAA Paper 92-3249, July 1992.

21. Pratt, D.T., and Heiser, W.H., "Isolator-Combustor Interaction in a Dual-Mode Scramjet Engine," AIAA Paper 93-0358, January 1993.

22. Zucrow, M.J., and Hoffman, J.D., *Gas Dynamics*, Vol. I, John Wiley and Sons, NY, 1976, pp. 206-210.

23. Sutton, G.P., *Rocket Propulsion Elements*, John Wiley and Sons, NY, 1986, pp. 54-55.

24. Summerfield, M., Foster, C.R., and Swan, W.C., "Flow Separation in Overexpanded Supersonic Exhaust Nozzles," *Jet Propulsion*, Vol. 24, No. 5, 1954, pp. 319-321.

25. Crocco, L., "Considerations on the Shock-Boundary Layer Interaction," *Proceedings of the Conference on High-Speed Aeronautics*, Polytechnic Institute of Brooklyn, NY, 1955, pp. 75-112.

26. Bogdonoff, S.M., and Kepler, C.E., "Separation of a Supersonic Turbulent Boundary Layer," 22nd Annual Meeting of the I.A.S., NY, January 26, 1954.

27. Soetrisno, M., and Imlay, S.T., "Simulation of the Flow Field of a Ram Accelerator," AIAA Paper 91-1915, June 1991.

28.   Srulijes, J., Smeets, G., Seiler, F., "Expansion Tube Experiments for the Investigation of Ram-Accelerator-Related Combustion and Gasdynamic Problems," AIAA Paper 92-3246, July 1992.

Appendix A. Experimental Results

Table A1: Chromatograph Analysis and Projectile Velocities

| HS | Figure Label | Hand Reg. Settings | | | Chromat. Analysis | | Vtrans (m/s) | Unst./Fall Drive Out | Velocity (m/s) |
		O2	CH4	N2	CH4	N2			
999	2d	2.00	2.82	5.40	2.86	5.45	1392	Unst	2051
1000	2e	2.00	2.82	5.20	2.86	5.21	1411	Unst	2073
1001	3a	2.00	2.82	4.50	Sample	Lost	1389	Unst	1861
1002	3c	2.00	2.82	4.00	2.95	3.99	1406	Unst	1817
1003	4b	2.00	2.82	3.00	2.99	3.04	1363	Unst	1416
1004	2 f	2.00	2.82	4.80	2.90	4.73	1382	Unst	2122
1005	3d	2.00	2.82	3.66	2.92	3.72	1384	Unst	1754
1006	4a	2.00	2.82	3.33	2.91	3.31	1384	Unst	1471
1007	No Ign.	2.00	2.82	6.50			1124	Unst (Kant)	941
1008	2c	2.00	2.82	6.50	2.89	6.47	1399	Unst	1947
1009	1a	2.00	2.82	12.00	2.82	11.63	1387	Fall Off	1428
1010	Ign. Prob.	2.00	2.82	9.00	2.87	9.03	N/A	Unst	1307
1011	Ign. Prob.	2.00	2.82	9.00	2.78	8.93	N/A	Unst	1254
1012	1b	2.00	2.82	9.00	2.80	8.80	1384	Fall Off	1411
1013	2b	2.00	2.82	7.50	2.82	7.45	1382	Unst	1896
1014	2a	2.00	2.82	8.20	2.83	8.10	1394	Drive Out	1848
1015	Nominal	2.00	2.82	5.66	2.86	5.55	1414	Unst	1937
1016	Nominal	2.00	2.82	5.66	2.86	5.56	1555	Unst	2046
1017	5b	2.00	2.82	4.65	2.87	4.62	1519	Unst	1928
1018	5d	2.00	2.82	4.25	2.89	4.19	1540	Unst	1638
1019	5a	2.00	2.82	5.00	2.81	4.96	1549	Unst	2057
1020	5e	2.00	2.82	3.83	2.89	3.77	1540	Unst	1793
1021	5c	2.00	2.82	4.50	2.83	4.44	1552	Unst	1689
1022	3b	2.00	2.82	4.25	2.86	4.20	1409	Unst	1937
1023	5 f	2.00	2.82	3.33	2.83	3.33	1564	Unst	1676
1024	5g	2.00	2.82	3.00	2.92	3.03	1543	Unst	1569
1025	6b	2.00	2.82	3.84	2.94	3.88	1513	Drive Out	1659
1026	6c	2.00	2.82	3.00	Sample	Lost	1547	Unst	1583
1027	6a	2.00	2.82	3.00	2.94	3.01	1318	Coast Out	1100
1028	6d	2.00	2.82	3.00	2.92	3.04	1753	Unst	1800